Bioconjugate Chemistry

Review

pubs.acs.org/bc

Use of Nanoparticle Contrast Agents for Cell Tracking with Computed Tomography

Johoon Kim,[†,‡] Peter Chhour,[†,‡] Jessica Hsu,[†,‡] Harold I. Litt,[†,§] Victor A. Ferrari,[§] Rachela Popovtzer,[∥] and David P. Cormode*[,†,‡,§]

[†]Departments of Radiology, [‡]Bioengineering, Medicine, and [§]Division of Cardiovascular Medicine, Perelman School of Medicine of the University of Pennsylvania, 3400 Spruce Street, 1 Silverstein, Philadelphia, Pennsylvania 19104, United States

[∥]Department of Engineering, Bar-Ilan University, Ramat Gan, 5290002, Israel

ABSTRACT: Efforts to develop novel cell-based therapies originated with the first bone marrow transplant on a leukemia patient in 1956. Preclinical and clinical examples of cell-based treatment strategies have shown promising results across many disciplines in medicine, with recent advances in immune cell therapies for cancer producing remarkable response rates, even in patients with multiple treatment failures. However, cell-based therapies suffer from inconsistent outcomes, motivating the search for tools that allow monitoring of cell delivery and behavior in vivo. Noninvasive cell imaging techniques, also known as cell tracking, have been developed to address this issue. These tools can allow real-time, quantitative, and long-term monitoring of transplanted cells in the recipient, providing insight on cell migration, distribution, viability, differentiation, and fate, all of which play crucial roles in treatment efficacy. Understanding these parameters allows the optimization of cell choice, delivery route, and dosage for therapy and advances cell-based therapy for specific clinical uses. To date, most cell tracking work has centered on imaging modalities such as MRI, radionuclide imaging, and optical imaging. However, X-ray computed tomography (CT) is an emerging method for cell tracking that has several strengths such as high spatial and temporal resolution, and excellent quantitative capabilities. The advantages of CT for cell tracking are enhanced by its wide availability and cost effectiveness, allowing CT to become one of the most popular clinical imaging modalities and a key asset in disease diagnosis. In this review, we will discuss recent advances in cell tracking methods using X-ray CT in various applications, in addition to predictions on how the field will progress.

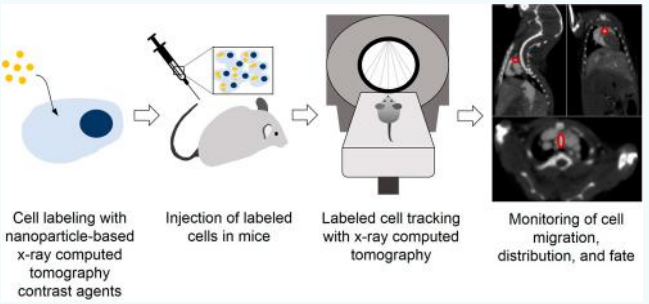

INTRODUCTION

CT was first developed in the 1960s and early 1970s by Godfrey Hounsfield and Allan McLeod Cormack, for which they were jointly awarded the Nobel Prize in Medicine in 1979.[1,2] Since then, CT has become one of the most widely used imaging modalities in medicine due to its wide clinical availability, low cost, and fast temporal resolution. CT's inherent ability to generate strong contrast between air, soft tissues, and bones facilitated its wide use in bone and lung imaging without the need for contrast agents. However, the use of FDA approved CT contrast agents, such as iodine-based small molecules and barium suspensions, extends CT's use for vascular imaging (e.g., diagnosis of pulmonary emboli, vascular calcifications, and hemorrhage) and digestive tract imaging. According to the Organisation for Economic Co-operation and Development, the number of CT exams increased from 78.9 per 1000 inhabitants in 1995 to 245 per 1000 inhabitants in 2015 in the U.S. alone.[3]

The development of novel contrast agents may continue this expansion in CT imaging usage. Recent advances in nanotechnology have produced novel nanoparticle CT contrast agents of various materials and structures.[4−11] Synthetic control over the size and shape of these contrast agents can determine pharmacokinetics and biodistribution, and facile surface modification enables loading of multiple cargoes for therapeutic efficacy and multimodality imaging.[6,12,13] Furthermore, owing to recent developments in CT scanners and reconstruction algorithms, the role of CT in medicine is expected to grow even larger.[14,15]

One of these growth areas for CT is in noninvasive cell tracking. This technique uses transplanted cells, often for cell-based therapies, which are labeled with exogenous contrast agents or reporter genes to enable visualization of the cells in vivo. Since cell tracking allows real-time and noninvasive monitoring of transplanted cells, it can be a powerful tool for evaluation of preclinical studies of new cell-based therapies, design of clinical trials, and monitoring of these therapies in clinical practice.[16]

In the following sections, we will review current applications of cell tracking and cover the different imaging modalities and labels that are used for cell tracking. We will outline the basic principles of CT and briefly introduce small molecule-based

Received: April 8, 2017
Revised: May 4, 2017
Published: May 9, 2017

DOI: 10.1021/acs.bioconjchem.7b00194
Bioconjugate Chem. XXXX, XXX, XXX−XXX

and nanoparticle-based CT contrast agents. We will then focus on recent studies of nanoparticle CT cell tracking in various applications and cell types, as well as studies on optimization of cell labeling. We will finally discuss the challenges that nanoparticle CT cell tracking faces and offer future perspectives on the field.

CELL TRACKING

Applications of Cell Tracking. Cell-based therapies have gained significant interest for their potential therapeutic effects in diseases that conventional medicine struggles to cure, such as cancer and neurogenerative diseases. For example, engineered chimeric antigen receptor T-cell therapy is close to clinical approval as a cancer treatment for B-cell malignancies and others.[17] However, the mechanisms of such disease treatments and behavior of transplanted cells are not well understood. Indirect monitoring from histopathology or other ex vivo biomarker analyses provides incomplete information on the status of transplanted cells from the point of injection until the end-point of the study, highlighting the need for direct monitoring using cell tracking methods that can provide essential information on the transplanted cells, such as their migration, distribution, and functionality.[18]

Cell tracking uses noninvasive imaging modalities to monitor cell movement and behavior in vivo after transplantation. Immune cells, stem cells, and cancer cells are the principal types that have been studied for their behavior in cell-based therapy and/or their role in disease progression.[19−22] With growing interest in immunotherapy and stem cell therapy, cell tracking methods will continue to be an important tool to expedite cell-based therapy development for clinical use.

Stem cell therapies have great potential in regenerative medicine because of their inherent biological properties of plasticity, self-renewal, and migration.[23] Stem cells have been tested frequently in diseases of organs that have limited regenerative capabilities, such as the central nervous system (CNS) and cardiac muscle, as seen from treatment of ischemic and stroke models of CNS injury.[24−26] Therapeutic benefits from neural stem cells are especially exciting as they can potentially offer a cure to neurodegenerative diseases for which no current cures are available, such as Parkinson's diseases and multiple sclerosis.[27−29] Various cell types, such as embryonic, adult, and induced pluripotent stem cells, can be used to restore damaged and injured tissue for therapeutic applications. The need for cell tracking in such applications is reinforced due to the complex nature of the CNS and cardiovascular system. To reach optimal therapeutic efficacy, it is important for administered stem cells to survive, migrate and home to the site of interest, and differentiate into the desired cell lineages. These post-transplantation cell behaviors are heavily dependent on the cell type, dose, and mode of administration, which can be determined and adjusted using the real-time monitoring afforded by cell tracking.[30] Safety issues related to stem cell therapy also create a need for monitoring. There is potential for serious adverse effects, such as teratoma formation, organ damage, graft failure, and malignant transformation.[23] Therefore, monitoring of transplanted cells in vivo by cell tracking methods will play a crucial role in understanding the safety and efficacy of stem cell therapy.

Another rapidly growing field in cell-based therapy is the use of immune cells for immunotherapy. Typically, immune response is induced in the patient by introducing immune cells that present antigenic peptides or by reintroducing autologous T cells that were harvested and expanded ex vivo.[31] For sustained and sufficient immune response, many components of the immune system, such as effector T cells, natural killer cells, and dendritic cells, need to work in a well-coordinated fashion in close proximity.[31] As with stem cell therapy, it is important to be able to track the transplanted cells continuously to understand the mechanism and efficacy of immunotherapy. Serial histology after multiple biopsies at different time points is currently used,[32] but it does not accurately represent the cell fate in vivo. Labeling immune cells with contrast agents will allow long-term observation of cell trafficking, distribution, and immune response induction to provide insight into therapeutic efficacy.[33,34] Adoptive immune cell therapy against cancer is a rising field in immunotherapy with a number of promising results already reported.[35,36] For example, T lymphocytes and dendritic cells are used for treatment of different malignancies. Cell tracking will allow real-time monitoring of distribution of the cells and persistence of immune response against tumors to assess therapeutic efficacy and facilitate advancement of cancer immunotherapies.

In addition, a treatment proposed for type I diabetes involves a cell-based approach in which microencapsulated pancreatic islet cells are delivered.[37] Microencapsulation of these transplanted islet cells into semipermeable alginate gels allows oxygen, nutrients, and insulin to pass through while inhibiting access of antibodies and immune cells to the islet cells, preventing immune rejection. Cell tracking methods allow monitoring of distribution, persistence, and engraftment of the microcapsules to ensure long-term treatment.[38]

Cell tracking can also provide great insight into cancer cell behaviors. Cancer cell lines such as A549 lung cancer[39] and UM-UC-3 human transitional cell carcinoma[40] have previously been labeled to study cancer development and metastasis. Cell tracking can be useful in understanding behaviors of cells with migratory characteristics, especially toward disease sites, to analyze their roles in disease progression and develop effective therapies in response.

Direct Cell Labeling. To allow noninvasive tracking of transplanted cells with imaging modalities, cells first need to be labeled in such a way that allows their visualization. A common approach to label cells is to incubate them with contrast agents in vitro prior to transplantation, a process called ex vivo direct cell labeling. The labeling agents are either internalized by the cells via endocytosis or phagocytosis or attached to the surface of the cells. The labeled cells are then purified from excess label and other reagents, before being injected into the subject. For successful in vivo imaging, it is crucial to achieve sufficiently high cell labeling to allow their detection. Furthermore, greater detection sensitivity is often advantageous; thus transfection agents, antibodies, or electroporation are often used to enhance cellular uptake.[16,30] The labeling agents can also be directly injected into the subject, in a process called in situ direct cell labeling; however, this approach suffers from uptake by nontarget cells and much higher dosage requirements than in vitro labeling.[30]

Indirect Labeling. Direct cell labeling is a simple and straightforward method, but this approach has several drawbacks. First, direct labeling provides no information on the viability of cells. Furthermore, if the cells die, the label may be retained at the target site, being taken up by macrophages, for example, leading to erroneous conclusions about the presence of cells. The labels may also become dissociated from the cells through efflux and exocytosis, leading to false quantification and

DOI: 10.1021/acs.bioconjchem.7b00194
Bioconjugate Chem. XXXX, XXX, XXX−XXX

monitoring of free labels instead of the cell of interest.[16,23] Second, cell division dilutes the number of labels, which reduces the sensitivity for detection of daughter cells, limiting long-term tracking of labeled cells.[41] Asymmetrical divisions of stem cells can be especially problematic for cell tracking, since some of the administered cells can no longer be detected after just one cell division.[41]

Indirect labeling addresses some of the problems of direct labeling using genetic modification of the cells. By placing reporter genes in the promotor region of other genes, labels such as enzymes, receptors, or proteins are expressed for long-term tracking of the cell.[16,23,42] The reporter genes can be transferred to the cell with viral agents or nonviral agents, such as liposomes, polymers, and transfection agents. Since the reporter genes are transcribed only in live cells, it is also possible to distinguish live cells from dead cells and monitor cell proliferation. The limitations of this approach include issues of stably expressing the genetic label in the cells and concerns over the safety of using genetically modified cells in patients.[16]

IMAGING MODALITIES AND CONTRAST AGENTS IN CELL TRACKING

Magnetic Resonance Imaging (MRI). MRI is one of the most widely studied imaging modalities for noninvasive cell tracking applications. MRI offers good spatial resolution and soft tissue contrast and does not involve exposure to ionizing radiation; however, its shortcomings involve slow acquisition times and relatively poor sensitivity toward contrast agents, as well as the contrast produced having a complex dependency on agent concentration. Various types of MRI contrast agents have been developed, such as iron oxide nanoparticles and gadolinium chelates. Superparamagnetic iron oxide nanoparticles (SPIO) are the most widely used class of MRI contrast agent used for cell tracking due to their biocompatibility and biodegradability. The first clinical study of MRI cell tracking with SPIO showed accurate detection of the number of lymph nodes injected with dendritic cells.[43] MR tracking also revealed misguided injection of dendritic cells that was not detected using either radionuclide imaging or ultrasound guidance, showing the value of MRI cell tracking. However, there are problems associated with SPIO-based MRI cell tracking, such as difficulty tracking in tissues with high iron content (e.g., hemorrhage sites),[16,23,41] and obscuring of underlying tissue anatomy in areas of images with high cell content.

Optical Imaging. Optical imaging, which encompasses techniques such as fluorescence and bioluminescence imaging, can be a powerful tool in cell tracking due to quick image acquisition times, low risk of toxicity, high temporal resolution and sensitivity up to 10^{-12} M, and low cost compared to MRI and PET imaging.[44] However, the primary disadvantage of optical imaging is its low depth penetration of only a few millimeters, as light is absorbed and scattered in tissue, limiting its potential application in human clinical research, as well as in small animals.[31] Another concern over fluorescence imaging is that the widely used fluorophores, such as cyanine dyes,[23] can suffer from photobleaching, limiting the ability to perform long-term tracking of cells. To address fluorophore photobleaching, semiconductor, light emitting, inorganic nanocrystals called quantum dots (QD) have been developed. Although cell tracking studies using QD have shown highly sensitive detection for prolonged durations, the cores of QD often contain cadmium or other heavy metals, creating concerns over long-term safety[30] and hindering applications in clinical studies. For indirect labeling for cell tracking with fluorescence imaging, fluorescent proteins such as green fluorescent protein (GFP) are used. For cell tracking with bioluminescence imaging (BLI), cells are transfected with proteins such as luciferase, and the substrate is administered at the time of imaging.

Radionuclide Imaging. Radionuclide imaging, i.e., positron emission tomography (PET) and single-photon emission computed tomography (SPECT), uses positron-emitting and gamma ray-emitting radioisotopes. The main advantage of radionuclide imaging in cell tracking is its high sensitivity; both SPECT and PET can detect labels with nanomolar to picomolar sensitivity.[45,46] Nuclear imaging thereby allows signal detection with very small amounts of labels, minimizing disruption of labeled cell function, as well as the surrounding tissue. The disadvantages of nuclear imaging include slow image acquisition times, low spatial resolution, exposure to ionizing radiation, and a lack of anatomic information. It is very common for nuclear imaging to be done together with another modality such as MRI or CT to provide anatomical registration.[47,48] The most widely used labels include ^{64}Cu-PSTM and ^{18}F-FDG for PET imaging and ^{111}In-oxine and ^{99m}Tc-HMPAO for SPECT imaging.[23] Possible adverse effects caused by cell radiation exposure, loss of the label, and limited ability to perform longitudinal studies due to eventual loss of signal from label decay are all drawbacks of such approaches.[49] A substantial number of reporter genes for SPECT and PET imaging have been developed. The most commonly used reporter genes for radionuclide imaging is the Herpes simplex virus thymidine kinase type 1 (HSV1-tk). The feasibility of cell tracking with indirect labeling for radionuclide imaging has already been shown in human;[50] however, there remains concern over possible immune response against nonhuman reporter genes.

Photoacoustic (PA) Imaging and Ultrasound Imaging. PA imaging, which is often done in conjunction with ultrasound, is another technique that can be used for cell tracking applications. PA imaging can reach submillimeter spatial resolution at lower penetration depth and can have up to 15 cm of penetration depth at lower spatial resolution.[51] For strong signaling, ideal PA contrast agents possess high molar extinction coefficients, sharp absorption peaks in the near-infrared window, high photostability, and efficient conversion of absorbed light into heat energy.[52] A good example of a class of contrast agents with such properties is AuNP, which have been used to track MSCs with PA imaging.[53,54] Ultrasound imaging alone also has been used for noninvasive cell tracking with gas-filled microbubbles as contrast agents.[55,56]

CT CELL TRACKING

CT has recently emerged as an imaging modality for cell tracking applications due to its appealing characteristics for those applications. CT has no depth penetration limit, has fast temporal resolution, is relatively low cost, and provides quantitative information on contrast agents in vivo. CT cell tracking also has substantial clinical potential as CT scanners are widely available in hospitals and research facilities. Recent developments in CT detectors,[15] reconstruction algorithms,[14] and contrast agents[57] have improved the sensitivity of CT, which has been an issue for using CT for cell tracking. In addition, the development of cell tracking for CT is a novel technological development for the cell tracking field. In this section of the review, the basic principles of CT and CT

DOI: 10.1021/acs.bioconjchem.7b00194
Bioconjugate Chem. XXXX, XXX, XXX−XXX

contrast agents will be presented. Then, recent studies on CT cell tracking for microencapsulated cells, tumor cells, stem cells, and immune cells, as well as studies of optimization of cell labeling, will be introduced.

CT Principles. A typical CT scanner has an X-ray source that emits a beam of photons toward the opposite side of the scanner, where an array of detector modules is positioned to absorb transmitted X-ray photons. Subjects are placed on a bed that moves into the scanner as the source and the detector rotate around the subject to collect 360° data sets. X-rays are generated in the source when electrons accelerated from a cathode collide with a metal anode, resulting in Bremsstrahlung and characteristic radiation. In Bremsstrahlung radiation, the accelerated electrons interact with the nuclei of the anode and lose some of their kinetic energy via X-ray photon emission (Figure 1A). In characteristic radiation, the incident electron

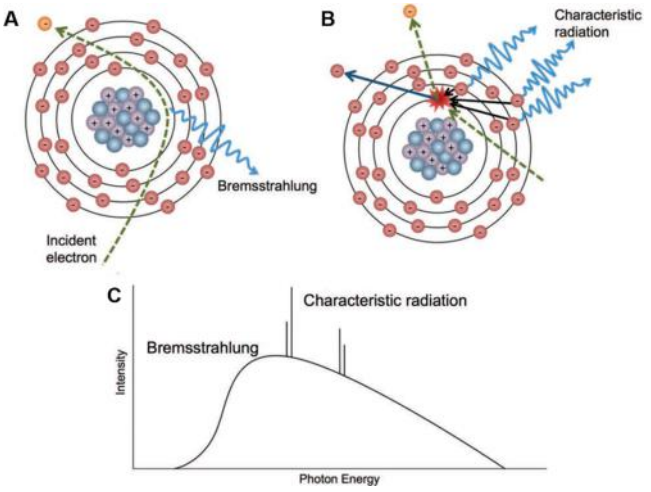

Figure 1. Schematic depictions of (A) Bremsstrahlung radiation and (B) characteristic radiation. (C) Typical photon energy spectrum emitted from a CT scanner. Figure reproduced with permission from ref 58.

collides and ejects an inner electron of the anode atom. Subsequently, an electron from an outer orbital fills the vacancy while emitting some of its energy as X-ray photon (Figure 1B). Due to the fixed energy difference between outer orbitals and the inner orbital, this results in sharp peaks in the X-ray spectrum (Figure 1C). The X-rays emitted from the tube are directed at the subject, where some of the beam is absorbed and scattered, while the remainder continues toward the detector.

The loss of X-ray intensity from absorption and scattering by the patient is referred to as X-ray attenuation. X-rays are attenuated by three types of interactions, namely, Compton scattering, the photoelectric effect, and coherent scattering. At the typical energy levels used in CT scans, the photoelectric effect and Compton scattering are the two main forms of interactions that cause attenuation.[57,58] The photoelectric effect occurs when incident X-rays collide with and transfer their energy to inner shell electrons (otherwise known as the K-shell), ejecting them from the atom as a result (Figure 2A). An electron from outer electron shell fills the vacancy and releases a photon, whose energy is characteristic to the atom.

The probability of the photoelectric effect occurring is generally proportional to Z^3 (Z = atomic number), explaining the considerable research interest in developing CT contrast agents based on high-Z elements. Note that the photoelectric

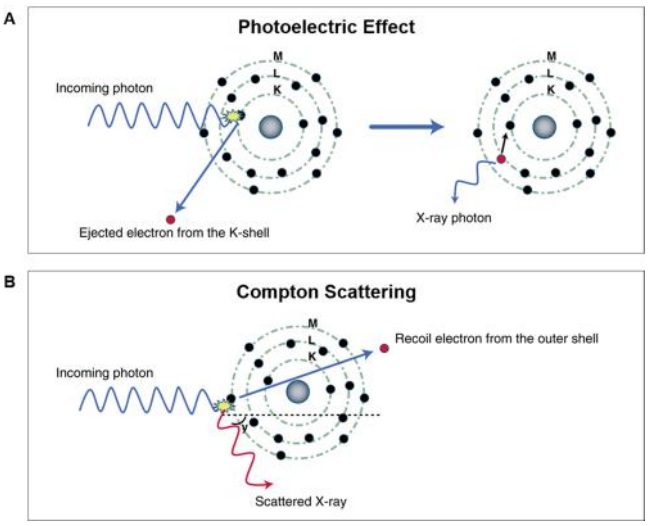

Figure 2. Schematic depictions of (A) the photoelectric effect and (B) Compton scattering. Figure reproduced with permission from ref 59.

effect can only occur above the binding energy of the K-shell electrons. In addition, the probability of such an event is maximal at the energy of the K-shell and declines as the energy increases beyond the K-shell, creating features in element X-ray attenuation spectra known as K-edges (Figure 3).

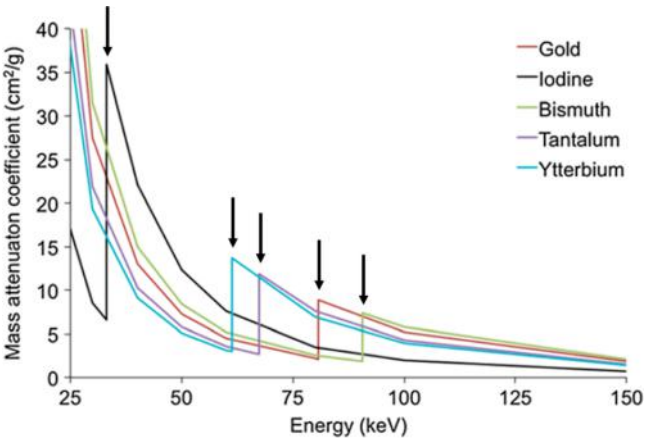

Figure 3. Mass attenuation coefficients of various elements where the K-edges are clearly apparent (spikes in the attenuation coefficient curves at certain energies indicated by down arrows). Figure reproduced with permission from ref 57.

In Compton scattering, incident X-ray photons interact with weakly bound electrons in the outer shell, lose some of their energy, and are deflected from their original path with reduced energy (Figure 2B). The deflection from their original path, as well as the use of collimation at the detectors, mean that Compton scattering is a cause of attenuation. Since Compton scattering occurs between photons and outer electrons, it is primarily affected by the electron density of the atom.[58]

CT attenuation is given in Hounsfield units (HU). For a given material X,

$$HU = 1000(\mu_X - \mu_{water})/(\mu_{air} - \mu_{water})$$

where μ is the attenuation coefficient. Air therefore has a CT attenuation number of −1000 HU and the attenuation number of water is 0 HU. The attenuation of bone ranges from 400 to

DOI: 10.1021/acs.bioconjchem.7b00194
Bioconjugate Chem. XXXX, XXX, XXX−XXX

1000 HU, and most soft tissues have attenuation of about 40 to 80 HU.[57] The energies and number of X-rays in the beam depend on the maximum tube voltage and electric current used. The maximum photon energy is equivalent to the maximum tube voltage, and the number of photons is inversely proportional to the energy (except at the characteristic energies of the anode material). However, low-energy X-ray photons are easily absorbed in the anode and filters made of materials such as aluminum are placed between the anode and the patients, eliminating X-rays in the 0−25 keV range and reducing the number of X-rays in the 25−50 keV range (Figure 1C). In addition, absorption of lower energy photons within the patient can occur, creating an effect known as beam hardening.

The source and detector array are positioned opposite to each other and rotate 360° around the subject to collect attenuation data from all angles.[57] In a typical CT scanner, most Compton-scattered X-rays are absorbed in a collimator positioned in front of the detector. The collimated X-ray radiation is absorbed, and its energy is converted to light in each pixel of a scintillator. The generated light energy in each pixel is then converted into current, which is converted into a digital value. Digital output from each detector module is collected and serialized for transmission.[60] From the transmitted data, CT images are reconstructed using computer algorithms. Filtered back-projection algorithms have traditionally been used for reconstruction. However, with recent advancements in computing power, iterative reconstruction methods have been applied, which result in noise reduction and hence improvement in sensitivity (Figure 4).[14,61]

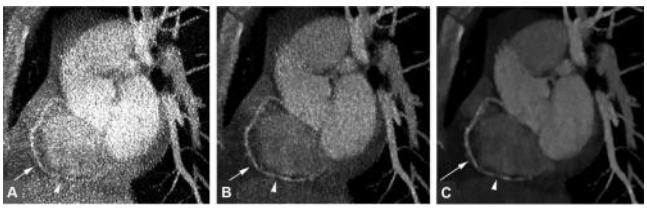

Figure 4. Images of coronary computed tomography angiography of the right coronary artery reconstructed with (A) filtered back projection, (B) hybrid iterative reconstruction (iDose^4), and (C) iterative model based reconstruction. The white arrow points at the right coronary artery, and the white arrowhead points at a noncalcified plaque. The images demonstrate noise reduction of iterative reconstruction when compared to filtered back projection. Figure reproduced with permission from ref 61.

Post-processing parameters including windowing, slice thickness, and field of view can be adjusted to give optimal image appearance and spatial resolution.[62] Recent improvements in detector rows, gantry rotation speed, reconstruction methods, and 3D rendering image processing make CT a powerful tool for diagnostic purposes. Furthermore, recently developed CT systems that use photon-counting detectors can provide energy resolution of the detected photons, which allows differentiation of multiple tissues and contrast agents (Figure 5).[63−65] In order to provide more information in CT imaging, contrast agents are often used. With photoelectric effect and K-edge attenuation taken into consideration, elements with high atomic number and appropriate K-edge energy (i.e., K-edges where there are high numbers of photons in the energy distribution in Figure 1C) have good potential to be used as CT contrast agents.

Small Molecule CT Contrast Agents. While CT alone is excellent for imaging the skeleton, calcified tissue (e.g., kidney stones), the lungs, and other structures, it is hard to distinguish soft tissues via CT scans without contrast agents since they have very small differences in X-ray attenuation. For better delineation of blood vessels and other organs, injections of exogenous compounds as contrast agents are used. The most widely used compounds in clinical settings are barium sulfate suspensions, which are limited to GI tract imaging, and iodinated molecular contrast agents, which are used both orally and intravascularly.[66,67] Iodinated contrast agents have been used since the 1950s,[68] and most currently used iodinated contrast agents are nonionic derivatives of 1,3,5-triiodobenzene, such as iohexol, which has three amide and six alcohol substituent groups that provide water solubility, biocompatibility, and low osmolality.[57] These iodinated contrast agents are nonspecific and suffer from low contrast generation due to their low payloads (only three contrast generating atoms per molecule) and have short blood circulation times, necessitating rapid post-injection imaging. Furthermore, their rapid clearance via the kidneys can result in renal damage in patients with kidney disease[69,70] and they cause adverse reactions in a subset of patients.[71] To overcome these limitations of small molecule iodinated contrast agents, there has been considerable recent interest in the development of alternative CT contrast agents.[57,58,72−74] Most of the novel agents reported in the past decade have been nanoparticle-based formulations.

Nanoparticle CT Contrast Agents. The detection limit of CT toward contrast agents is around 10^{-3} M, which is less sensitive than MRI ($\sim 10^{-5}$ M) or nuclear imaging ($\sim 10^{-10}$ M).[75] To overcome this low sensitivity, dense nanoparticles with high payloads are needed for CT molecular imaging applications. Further motivation for nanoparticle contrast agent development is the increasing number of patients with impaired kidney function, for whom the use of the current iodinated contrast agents is contraindicated.[76,77] Nanoparticles of 3 nm, for example, could contain hundreds of contrast generating atoms, which would place a lower burden on the kidneys since far few excretion events would be needed. Alternatively, nanoparticles can be designed to erode slowly, resulting in gradual release of their payload for excretion, minimizing the concentration at the kidneys at any given time.[4,5]

Nanoparticles are structures that are between 1 and 1000 nm in one or more dimensions. Most reported nanoparticles are approximately spherical, but they can have many other shapes, such as rods,[78] cages,[9] or stars.[79] The shape of a nanoparticle can strongly influence its properties; for example, the shape of a gold nanoparticle can determine its suitability for applications such as optical imaging or surface enhanced Raman spectroscopy.[78,80,81] Nanoparticle contrast agents for CT typically consist of a core loaded with contrast generating atoms, which is coated with polymers, lipids, proteins, silica, or other compounds that can provide the desired circulation times, biodistribution, biological media solubility, and biocompatibility. The coating layers can also usually be easily modified to incorporate other functionalities, such as target specificity with antibodies, therapeutic effects via drugs or nucleic acids, or multimodal imaging capacity with other contrast generating moieties.[12,82] Nanoparticles may therefore also be synthesized to possess desired magnetic or optical properties to provide versatility and multifunctionality.[30] Lipid-based structures (liposomes, emulsions, micelles, or lipoproteins) and solid core nanoparticles (metal, metal alloy, or metal salt) or combinations of the two are the most frequently studied formations for CT applications.[6,10,83] For metal core-based

DOI: 10.1021/acs.bioconjchem.7b00194
Bioconjugate Chem. XXXX, XXX, XXX−XXX

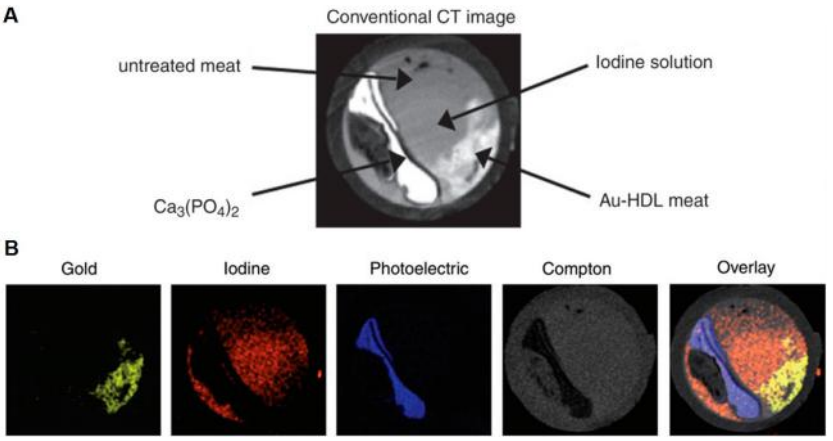

Figure 5. (A) Conventional CT image of an artery phantom. (B) Spectral CT gold, iodine, photoelectric, and Compton images of the phantom and an overlay of all four images. Figure reproduced with permission from ref 63.

agents, AuNP have been the most extensively studied as CT contrast agents, due to gold's high atomic number of 79 giving it a K-edge at 80.7 keV, its excellent biocompatibility, being inert in biological settings, synthetic control over size and shape, as well as ease of surface modification.[13,84] Other heavy metal elements, such as iodine, bismuth, bromine, tantalum, platinum, ytterbium, yttrium, gadolinium, and tungsten, have also been studied.[57,85,86]

Nanoparticles are most widely studied for vascular imaging as blood pool CT contrast agents since they can be engineered to have long circulation times.[6,85] They have also garnered significant research interest for cancer imaging via both passive and active targeting.[10,72] By conjugating various targeting moieties to nanoparticles, targeted imaging of lymph nodes and cardiovascular diseases have been demonstrated.[86] Nanoparticle CT contrast agents can also be used for concurrent diagnosis and therapy by loading therapeutic cargoes or by exploitation of inherent therapeutic properties, such as photothermal ablation using gold nanorods.[87]

Nanoparticles have been used for cell tracking applications with other modalities including MRI and SPECT, which allow tracking of many different cell types in various clinical applications,[43,88−91] and there has been growing interest in using CT contrast agent nanoparticles for cell tracking. In designing and selecting appropriate elements for nanoparticles for CT cell tracking, there are several criteria to take into consideration. First, the nanoparticles should be highly biocompatible (i.e., their uptake should not affect cell viability) and should not disrupt cell function, such as migration, cell surface marker expression, and response to stimuli. Second, the nanoparticles must maintain their physiochemical properties (i.e., minimal aggregation, dissolution, degradation) inside the labeled cells to prevent adverse effects on the cells. Third, the nanoparticles should deliver high payloads of contrast agent to allow detection of the administered cells. Gold nanoparticles (AuNP) have been the first choice for CT cell tracking to date due to their high density (d = 19.3 g/cm^3), stability, and excellent biocompatibility providing high payloads, sustained contrast, and lack of adverse effects on cells. However, there is potential for the use of many other elements as the basis for CT cell tracking contrast agents.

CT Cell Tracking Applications. *Microencapsulation.* While cell therapy has tremendous potential to treat diseases that current conventional medicines cannot effectively cure, the source of the cells can create challenges. For instance, autologous stem cells are scarce, and the patient might not have enough healthy cells to harvest and expand in numbers ex vivo. As an alternative, xenotransplantation and allotransplantation of cells can be used; however, immune rejection from the patient often jeopardizes the outcome of the therapy. To prevent immune rejection, patients can be given immunosuppressive drugs, but they can lead to serious complications, such as increased risk of infection and cancer.[92] A promising strategy to avoid immunorejection is microencapsulation of transplanted cells. In this strategy, cells to be transplanted are embedded in microcapsules made of hydrogels (most commonly made of alginate), which protects the cells and allows them to grow and function. These microcapsules are semipermeable, allowing nutrients (i.e., oxygen, glucose) and metabolites to pass through, but blocking immune cells and antibodies from interacting with the transplanted cells.[92] Alginate microcapsules have broad applications in cellular therapy, such as liver failure[93] and spinal cord injury.[94] However, the most widely studied application of microencapsulation is in treatment of type 1 diabetes mellitus, an autoimmune disease in which T-cells destroy insulin-producing beta cells. For this application, human islets are encapsulated in alginate microcapsules to produce insulin in the body without immune rejection. Since this concept was first introduced by Lim and Sun in 1980,[95] many preclinical and clinical trials have been launched, demonstrating considerable therapeutic efficacy in insulin regulation.[96,97] However, the success rate of engraftment varies, and the fate of the transplanted islets and subsequently the cause of variation in efficacy are poorly understood. Currently, the efficacy is indirectly evaluated with blood glucose level and C-peptide level measurements, which do not provide any information on the behavior of transplanted cells, such as their location and the persistence of their functionality. Thus, monitoring via noninvasive cell tracking techniques is highly desired to fully understand the fate of the transplanted islets. It will allow efficacy of engraftment to be monitored consistently and important parameters, such as mode of delivery, cell dose, and transplantation site, can be determined to optimize the therapy.[92] The large size of microcapsules enables incorporation of contrast agents in the shell around the cells, facilitating noninvasive monitoring with CT.

DOI: 10.1021/acs.bioconjchem.7b00194
Bioconjugate Chem. XXXX, XXX, XXX−XXX

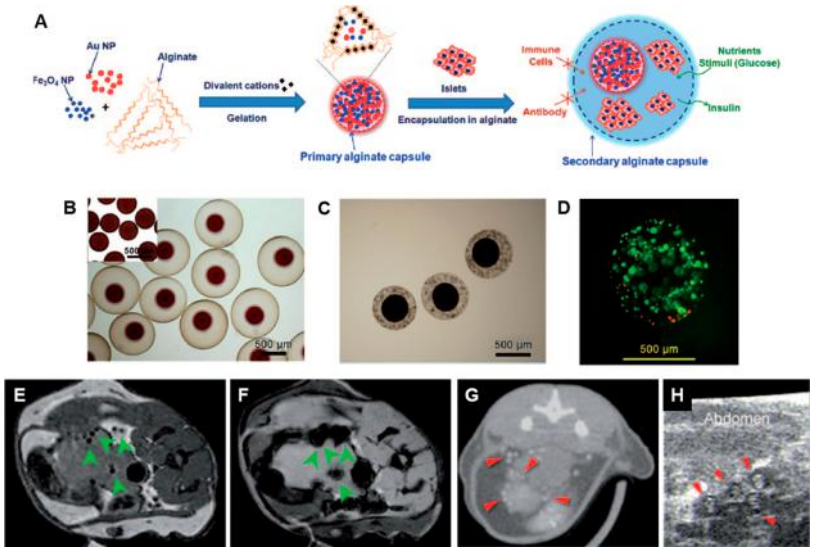

Figure 6. (A) Schematic depictions of CIC synthesis and structure. (B) Microscopy image of CIC without cell encapsulation. (C) Microscopy image of CIC with beta-TC6 mouse insulinoma cells encapsulated. (D) Fluorescence microscopy image of encapsulated mouse insulinoma cells. Green = live cells, red = dead cells. (E) Spin−echo MRI image, (F) gradient-echo MRI image, (G) micro-CT image, and (H) ultrasound image acquired 1 day after injection of 1200 CIC into the abdomen of a mouse. Figure reproduced with permission from ref 102.

During microcapsule synthesis, barium ions (Ba^{2+}) or calcium ions (Ca^{2+}) are used to cross-link alginate and form the capsules.[98] Barium ions are radiopaque, enabling visualization in CT without additional contrast agents.[99] Different parameters of the microcapsules, such as gelation time, concentration of polycation (i.e., protamine sulfate and poly(L-lysine) (PLL)), and type of outer layer alginate can be altered to improve their mechanical strength.[98]

As well as contrast arising from the cross-linking ions, other materials can be coencapsulated to provide additional contrast for other modalities or enhanced detection sensitivity. For example, Barnett et al. developed alginate microcapsules that contained perfluorocarbon (PFC) nanoparticles to improve cell function and enable multimodality imaging with CT, ultrasound, and MRI.[100] Fluorine and bromine in the PFC nanoparticles allow imaging with fluorine MRI and CT, respectively, and change in the local echogenicity by the microcapsules allows ultrasound imaging. The use of multiple imaging modalities can be valuable as the advantages of each modality can be harnessed, such as the excellent soft tissue contrast of MR, high spatial resolution of CT, and real-time imaging provided by ultrasound. The feasibility of using PFC nanoparticles for cell tracking with these three imaging modalities was already established by the same research group, using human pancreatic islets directly labeled with PFC.[101] The group also hypothesized that coencapsulation of PFC nanoparticles would have the additional benefit of increased oxygen flow to the islets, preventing necrosis, which is the main issue for microencapsulated islets. Capsules labeled with perfluoropolyether (PFPE) were imaged with ^{19}F MR imaging, while capsules labeled with perfluorooctyl bromide (PFOB) were imaged with ultrasound and CT imaging. Individual fluorocapsules could be detected by all three imaging modalities both in vitro and in vivo. Inclusion of PFC nanoparticles did not alter the permeability of the microcapsules, keeping the islets immunoprotected, and increased cell viability when compared to unlabeled microcapsules. More importantly, both types of fluorocapsules had enhanced glucose responsiveness and insulin secretion in vitro, and persistent insulin secretion in mice. When compared to direct PFC labeling,[101] microcapsules loaded with PFC nanoparticles gave improved cell viability and glucose responsiveness, indicating the potential of the microencapsulation method.

An alternative method to load nanoparticles in microcapsules has been explored for better cell viability and function maintenance. Kim et al. developed a "capsule-in-capsule" (CIC) structure that consists of a primary inner capsule containing nanoparticles (iron oxide and gold) within a secondary outer capsule that contains the therapeutic islet cells (Figure 6A−C).[102] The goal of using this structure was to prevent contact between the nanoparticles and the cells, thereby avoiding any potential adverse effects that the nanoparticles might cause the cells.

By encapsulating iron oxide and AuNP, CICs could be monitored with CT and MRI. The alginate microcapsules were also intrinsically detected in ultrasound imaging, allowing trimodal imaging. Using Ba^{2+} ions and higher alginate concentrations for the primary core, the integrity of the capsules was maintained, and subsequently, the physical separation of nanoparticles from the transplanted cells was preserved without release for at least 3 months in vitro. In vitro studies showed high cell viability (Figure 6D) and prolonged insulin secretion from embedded mouse insulinoma cells. Both in vitro and in vivo imaging results showed that single capsules could be identified by all three imaging modalities (Figure 6E−H). Injection of CICs in mice enabled imaging up to 3 months, and blood glucose levels were maintained in the normal range for at least 75 days.

The possibility of trimodal imaging (CT, MRI, and ultrasound) of microcapsules was further explored by Arifin et al.[37] In this study, AuNP functionalized with dithiolated diethylenetriaminepentaacetic acid (DTDTPA) were labeled with gadolinium chelates as contrast agents for CT and MRI.[37] The microcapsules could be detected with all three imaging modalities both in vitro and in vivo. Islet cell viability and functionality were not affected, which is further evidenced by lack of change in size, morphology, or leakage of nanoparticles.

DOI: 10.1021/acs.bioconjchem.7b00194
Bioconjugate Chem. XXXX, XXX, XXX−XXX

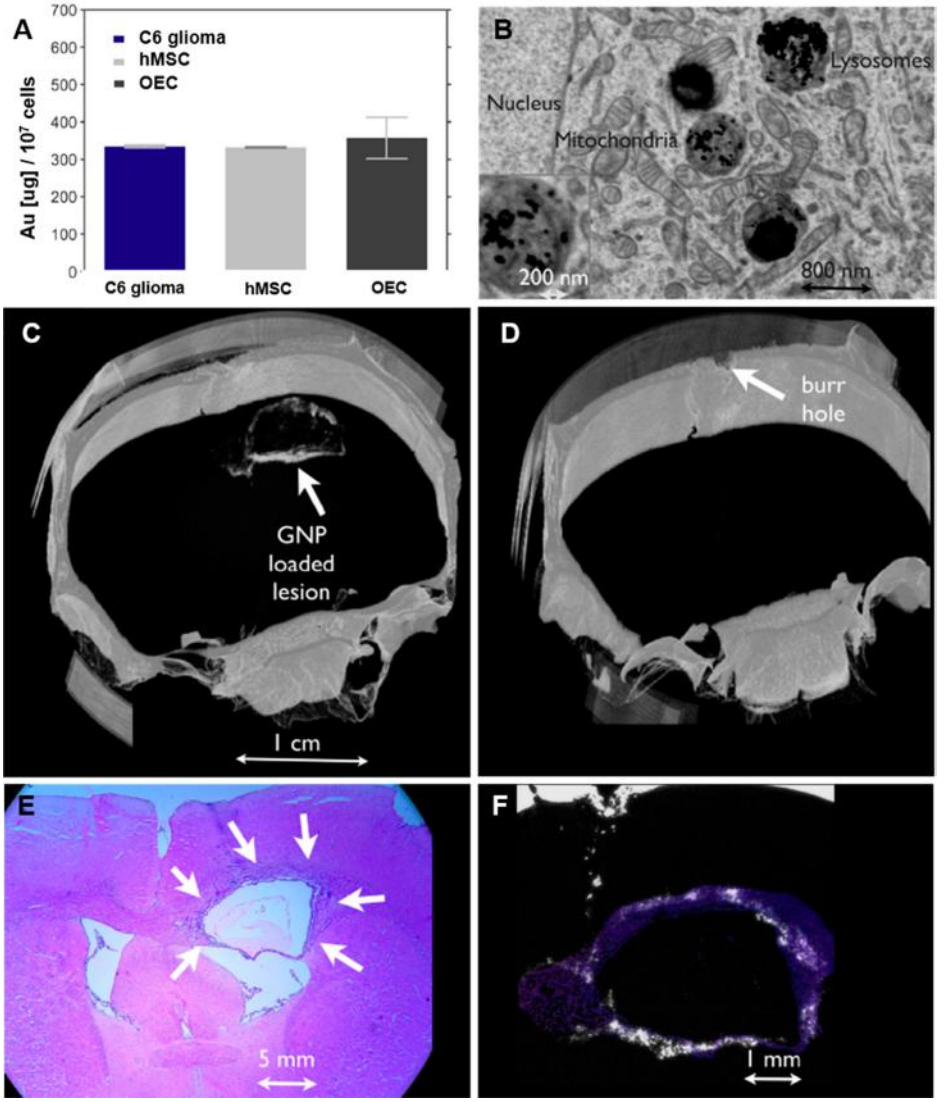

Figure 7. (A) Average gold uptake of 10^7 cells C6 glioma cells, hMSCs, and OECs after 22 h incubation with 52 μg/mL AuNP. (B) TEM of a glial cell showing AuNP uptake (black dots). (C,D) Synchrotron radiation source phase contrast CT image 14 days after injection of either (C) AuNP loaded glioma cells or (D) unlabeled glioma cells. (E) H&E histology image of the lesion. (F) Overlay of synchrotron radiation source phase contrast CT image and histology of the brain tumor. Figure reproduced with permission from ref 105.

More recently, Astolofo et al. used polymer-coated 60 nm AuNP and both synchrotron radiation and X-ray micro-CT imaging to track AuNP-loaded microcapsules.[99] The simple synthesis protocols of microcapsules and AuNP allow economical and rapid preparation of AuNP loaded micro-encapsules. AuNP loading did not affect the viability of cells in microcapsules. These microcapsules had good mechanical stability in vitro, remaining intact with no gold leakage even after 2 months of shaking (110 rpm at 37 °C). The structure was also preserved without AuNP escape after autoclaving (121 °C for 20 min). Post-mortem imaging in mice demonstrated that individual microcapsules could be detected. The above reports indicate the potential of cell tracking with the use of CT. However, most cell tracking applications do not use microencapsulated cells, but free cells. Therefore, for the broad utility of CT cell tracking to be shown, labeling of cells themselves needed to be developed, as will be described in subsequent sections.

Tumor Cell Tracking. Cell tracking is a useful tool in cancer research, since tumor cells migrate and spread within the body.[103] Tracking malignant cancer cells helps us better understand tumor development in its initial growth, progression, and metastatic spread; all of this information can be used to develop more effective antitumor therapies. CT imaging is used in cancer screening and monitoring; therefore cancer cell tracking with CT could be very useful. An early study of cell tracking using synchrotron CT was performed by Hall et al. with AuNP labeled C6 glioma cells.[104] The group demonstrated that it is possible to visualize individual clusters of approximately 3000 labeled glioma cells (average size of 150 μm) in the brains of rats, although the characteristics of the AuNP used in this study are not clear.

Tumor cell tracking with X-ray CT and AuNP was further developed by Menk et al.[105] Phase-contrast X-ray CT in the edge enhancement regime was used to obtain high resolution 3D images that could distinguish small cell clusters of less than 10 cells. 50 nm, horse-serum protein-coated AuNP were incubated with 10^7 of C6 glioma cells to achieve uptake of approximately 26 000 AuNP per cell in 22 h (Figure 7A). TEM images confirmed AuNP uptake within the cells since AuNP

DOI: 10.1021/acs.bioconjchem.7b00194
Bioconjugate Chem. XXXX, XXX, XXX−XXX

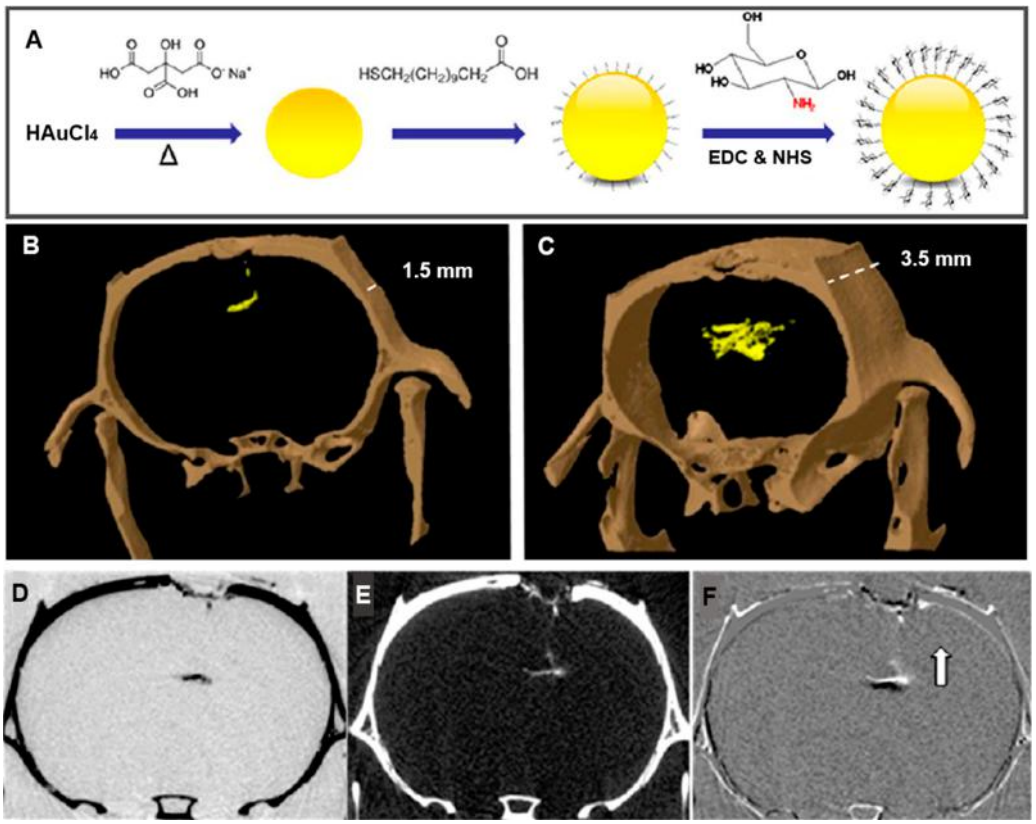

Figure 8. (A) Schematic depiction of the synthesis and structure of AuNP used for hMSC labeling. (B,C) 3D in vivo volume rendered micro-CT scans of rat brains acquired one month after injection with (B) labeled hMSCs and (C) free AuNP. (D–F) Coronal brain slice (D) 1 week post-transplantation, (E) 3 week post-transplantation, and (F) Overlay of D and E showing the migration pattern of the cells. Figure reproduced with permission from ref 111.

were seen to be localized in lysosomes in large aggregates (Figure 7B). In vitro experiments showed that there was no effect of AuNP loading on the viability and proliferation of the cells studied. For visualization of labeled tumor cells in vivo, synchrotron radiation source phase contrast CT imaging was performed (Figure 7C,D). When 600 000 C6 cells were implanted and allowed to grow into a tumor mass for 14 days, the total cell number in the tumor could be estimated by CT image segmentation (Figure 7C). The cell cluster reconstruction in high-resolution CT was found to overlay closely with histology results (Figure 7E,F). When 100 000 C6 cells were implanted and allowed to grow for 14 days, synchrotron radiation source phase contrast CT allowed the detection of infiltrations of cancer cells away from the main tumor bulk. Synchrotron radiation source phase contrast CT gave superior image quality with sharp lesion boundaries and clearer segmentation of the images when compared to other CT imaging techniques, such as synchrotron radiation attenuation CT and benchtop phase contrast micro-CT.

Tumor cell tracking using synchrotron CT and AuNP has also been demonstrated by Astolfo et al. using a mouse model of glioblastoma multiforme.[103] The group first used a 3D head model to estimate the required radiation dose from synchrotron CT in order to achieve sufficiently small pixel size for detection of small cell clusters. The estimate was used to visualize unorganized cell clusters of 100 to 150 μm in size 8 days after injecting 100 000 AuNP-labeled glioma cells in the brains of the mice.

The detection limit of AuNP-loaded tumor cells with synchrotron based CT was also studied by Schultke et al.[106] Synchrotron-based X-ray CT images of AuNP-labeled C6 glioma cells injected in the brain of Wistar rats were compared with small animal MRI. While the MRI images allowed easier distinction between the tumor and the surrounding soft tissue, the CT images visualized the morphological features of the bones and voids in the tumor more accurately. A large tumor could be seen around the implantation site, as well as a smaller second tumor, and even small cell clusters. Furthermore, quantitative image analysis allowed measurement of tumor volume and other characteristics. The results from CT correlated well with MRI and histology, supporting the utility of the CT for tumor cell tracking. The results described above, where AuNP labeled cells were imaged with synchrotron-derived or phase contrast CT, were highly promising; however, these techniques are not widely available and may be challenging to translate to a clinical setting. Therefore, the next hurdle to overcome for the field was to achieve tracking of labeled cells with conventional CT scanners.

Stem Cell Tracking. Stem cell therapy offers enormous potential for disease treatments in body parts with poor regenerative capabilities. Noninvasive cell tracking techniques are greatly needed to understand cell distribution, functionality, and safety of stem cell therapies. One of the earliest efforts to visualize stem cells using CT imaging was reported by Torrente et al.[107] Stem cells labeled with commercially available SPIO (Feridex, a dextran coated, ~150 nm nanoparticle[108]) were visualized using micro-CT after the cells were transplanted via

DOI: 10.1021/acs.bioconjchem.7b00194
Bioconjugate Chem. XXXX, XXX, XXX–XXX

intra-arterial infusion for muscle regeneration.[107] Iron oxide does not have very high X-ray attenuation or density. However, performing high resolution (1.65 μm), synchrotron source CT on 2 mm pieces of excised tissue compensated for this issue. This group aimed to track a systemically delivered subpopulation of human stem cells that expressed the CD133 antigen, detect their migration into the skeletal muscles of a muscular dystrophy mouse model,[107] and evaluate their contribution to muscle repair. Labeling CD133+ stem cells with these iron oxide nanoparticles did not disrupt their cell viability. When 10^6 labeled cells were injected via the femoral artery of the mice, the X-ray attenuation of labeled stem cells was significantly higher than the surrounding tissue of the injected leg. The group determined that cell numbers as low as 50 000 could be detected; however, quantification revealed that only 0.01% of injected cells migrated into the site of interest in the muscle. Menk et al. also reported imaging stem cell migration into disease sites.[105] In this study, U87 tumor cells were injected and allowed to grow into tumors in the brain for 7 days. After tumor development, AuNP labeled hMSCs were injected into the right carotid artery. Synchrotron radiation source phase contrast CT imaging at 24 h revealed localization of hMSCs in the tumor. Approximately 33% of the injected cells were found to migrate to the tumor site.

In addition to homing to tumors, hMSCs can also migrate and home to sites of injury and inflammation.[109] Furthermore, hMSCs have gained significant attraction as a cell source for therapy due to their easy isolation, rapid in vitro expansion, and capability of differentiating into multiple lineages.[110] Betzer et al. utilized these advantages of hMSCs for longitudinal hMSC tracking in the brain with conventional microCT imaging.[111] The study not only demonstrated noninvasive cell tracking with CT, but also highlighted the potential of stem cell therapy in treating neuropsychiatric disorders.[111] To label hMSCs, 20 nm core, glucose-coated AuNP were used (Figure 8A). After 10^6 cells were incubated with 30 μg/mL of gold for 3 h, approximately 1.1 million AuNP were internalized per cell. An MTT assay showed that the viability of the labeled cells was unaffected when examined for up to 8 days post-labeling.

A rat model of depression was used for in vivo studies, and labeled hMSCs were injected into the brains of the rats. In vivo scans showed that injected hMSCs could be tracked for up to 4 weeks. At 24 h after injection, cells were found to be dispersed from the injection site and appeared in a specific region after one month. This specific migration behavior of the AuNP labeled hMSC was distinctively different from free AuNP, in which the AuNP spread and scattered into many regions of the brain after one month (Figure 8B,C). This result supported the hypothesis that hMSCs navigate and home to regions of the brain involved in depression. The migration behavior was quantified by measuring number of voxels with gold and average density of the voxel over time. Over 3 weeks, the labeled hMSCs occupied fewer voxels, but their average density increased, and the opposite was found for free AuNP, indicating homing of hMSCs and retention of AuNP inside the cells (Figure 8D−F). Ex vivo imaging, quantification by flame atomic absorption spectroscopy and immunohistochemical staining all indicated that hMSCs substantially migrated into the cingulate cortex, which has been linked to depression.[112,113] The sucrose consumption test and forced swim test, measures of depression-like symptoms, showed that hMSC therapy attenuated depressive-like behavior in this rat model.

Meir et al. used the same glucose-coated AuNP for imaging and tracking of MSCs that are transplanted intramuscularly in a Duchenne muscular dystrophy mouse model. 10^6 MSCs were injected in the right limb of the mouse. CT scans performed over a period of 4 weeks demonstrated that with time the cells migrated from the injection site and spread in the muscle. Interestingly, the Duchenne muscular dystrophy animal model demonstrated the ability to image the anatomy and the pathology while simultaneously tracking the cells. Regarding the detection limit of the method, it was reported that as few as 500 Au-labeled cells could be detected, illustrating high sensitivity of CT in cell tracking.[114]

In a more recent study, Kim et al. coated AuNP with PLL and rhodamine B isothiocyanate (RITC) to visualize hMSCs in the brains of rats.[110] PLL was used as a cationic transfection agent to increase labeling efficiency since smaller non-phagocytic cells, such as hMSCs, do not readily take up nanoparticles. The AuNP coated with PLL (AuNP-PLL) did not aggregate, had a homogeneous size distribution of 40 nm in diameter, and were effectively internalized by hMSCs (up to ~600 pg/cell). Uptake of AuNP-PLL did not cause adverse effects on cell viability, proliferation, or adipocyte differentiation. Labeling was stable after 3 weeks in vitro, with cell dispersions providing strong attenuation in conventional microCT. This in vitro CT imaging indicated that CT contrast is proportional to the amount of internalized label and is linearly dependent on labeled cell number, highlighting the quantitative nature of CT imaging. In vivo studies demonstrated that cell numbers as low as 2×10^5 could be visualized in CT, which corresponded to a detection limit of approximately 2×10^4 cells per μL. Immunofluorescence microscopy was used to confirm the CT tracking results, showing similar distribution of a human cell marker and RITC (from AuNP labeled cells). The authors anticipate that CT tracking will be the most helpful in immediate imaging of cell distribution and verifying accuracy of cell delivery owing to its fast temporal resolution and wide availability in clinical environments. The studies by Betzer et al., Kim et al., and others below are notable since they are examples of cell tracking using conventional, polychromatic X-ray source CT systems, as opposed to synchrotron X-ray source systems. This is an important development, since polychromatic source CT systems are much more widely available in the laboratory setting and are the typically used CT scanners in the clinic.

Immune Cell Tracking. Immune cell tracking is of great interest for understanding mechanisms of diseases in which immune cells play a crucial role, such as atherosclerosis, arthritis, and ABCD syndrome. Furthermore, it can play an important role in improving immune cell-based therapy approaches. Immune cell-based therapy has been gaining significant attention as a novel approach for antitumor therapy.[35,36] However, the outcomes of human clinical trials have been mixed, indicating the potential need for cell tracking to evaluate cell behavior in the host after transplantation. To develop a novel method for immune cell tracking, Meir et al. used conventional X-ray CT and AuNP to track genetically engineered T-cells that are transduced to express melanoma-specific T-cell receptors.[115] These engineered T-cells were incubated with glucose-coated AuNP (the same formulation as described above in the Betzer et al. paper[111]) to achieve cell loading. In vitro IFNγ secretion upon coculture with target human melanoma cell lines was assessed to observe if labeling affected T-cell function. Incubations for 60 min at 0.7 mg/mL

DOI: 10.1021/acs.bioconjchem.7b00194
Bioconjugate Chem. XXXX, XXX, XXX−XXX

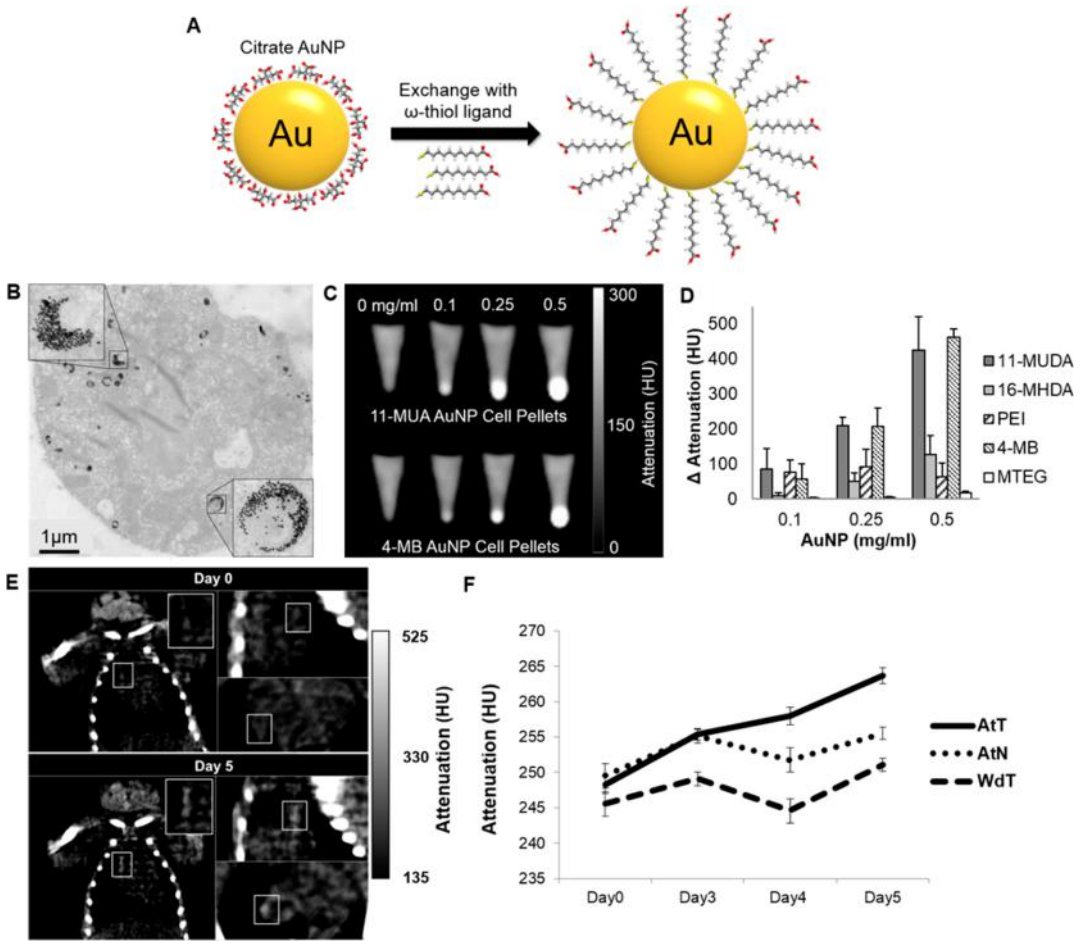

Figure 9. (A) Schematic depiction of ligand exchange with citrate capped AuNP. (B) TEM image of a monocyte cell after 24 h incubation with 11-MUA coated AuNP. (C) CT images of pellets of monocytes that had been labeled with 11-MUA and 4-MB. (D) Quantification of CT attenuation for each AuNP formulation. (E) CT scans of an atherosclerotic mouse before (day 0) and after (day 5) injection with gold labeled monocytes. The boxed area indicates aortic region of interest. (F) Average CT attenuation in the aortas of mice over the study period. Figure reproduced with permission from ref 116.

of AuNP were found to result in efficient labeling without disruption of cell function. For in vivo evaluation, the T-cells, also transfected with GFP, were injected intravenously into tumor-bearing mice. Substantial contrast was seen in conventional microCT imaging at the tumor sites after 24 h, and the signal reached its peak intensity at 48 h, illustrating migration of labeled T-cells to the tumor site. Quantitative image analysis indicated that about 460 000 cells migrated to the tumor site after 48 h. The CT images were compared to fluorescence imaging of GFP, which verified that the CT contrast observed was a result of tumor accumulation of the injected cells. The migration of engineered T-cells was further verified by enhanced tumor regression compared to control groups treated with nontargeted T-cells.

CT is widely used in the clinic for noninvasive imaging of the coronary arteries[116] due to its fast image acquisition avoiding cardiac motion artifacts and providing the high spatial resolution needed for these small structures. Since monocyte recruitment is an important process in atherosclerotic plaque progression, developing monocyte tracking for CT would be highly appealing. Chhour et al. used AuNP-labeled monocytes to track their migration into atherosclerotic plaques noninvasively using CT.[116] The importance of this study is highlighted by atherosclerosis development in the coronary arteries being the cause of the majority of deaths from cardiovascular diseases. Monocyte recruitment and its role in pathogenesis of coronary artery disease have been explored as a potential drug target for atherosclerosis regulation[117] and is the focus of studies in disease progression. In the Chhour et al. study, 15 nm AuNP were coated with a library of ligands (e.g., 11-mercaptoundecanoic acid (11-MUA), 16-mecaptohexadecanoic acid (16-MHA), poly(ethylenimine) (PEI), 4-mercapto-1-butanol (4-MB), 11-mercaptoundecyl-tetra(ethylene gycol) (MTEG) and others) to evaluate which coating provides nanoparticle stability in biological media without disrupting monocyte cell viability or function when internalized (Figure 9A). Transmission electron microscopy (TEM) images of the gold cores revealed spheres with average diameter of 14.6 nm in a narrow size distribution. Dynamic light scattering and zeta potential measurements were used to determine hydrodynamic diameter and surface charge, respectively, which confirmed ligand exchange. Incubations for 24 h with a monocyte cell line revealed that the AuNP formulations did not affect viability, except for PEI coated AuNP, at concentrations of up to 1 mg/mL. In vitro evaluation of TNF-α and IL-6 cytokine release from labeled monocytes showed that, with the exception of 4-MB coated AuNP, these AuNP did not affect cytokine release. TEM images of sections of monocytes after AuNP incubation

DOI: 10.1021/acs.bioconjchem.7b00194
Bioconjugate Chem. XXXX, XXX, XXX−XXX

indicate that AuNP localize in vesicles within the cells (Figure 9B).

In vitro CT imaging of labeled cell pellets showed that the highest CT attenuation and therefore cell uptake was achieved with 11-MUA and 4-MB coated formulations (Figure 9C,D). With the in vitro test results taken together, 11-MUA coated AuNP were chosen to be evaluated further, since they did not affect cell viability or cytokine release, and were highly taken up by monocytes. Primary monocytes were isolated from the spleens of donor mice and incubated with 11-MUA AuNP. Similarly favorable properties for cell labeling were observed in these cells; therefore in vivo experiments were initiated. Labeled primary monocytes were injected intravenously into a mouse model of atherosclerosis. The mice were imaged with CT over 5 days post-injection and attenuation in the aorta was found to increase during this time (Figure 9E,F). By day 5, there was an increase of 15.3 HU in the aortas of the atherosclerotic mice (AtT), which was significantly higher than the attenuation change in controls (i.e., unlabeled monocytes injected into atherosclerotic mice (AtN) and wild type mice injected with labeled monocytes (WdT)), indicating that recruitment of labeled monocytes could be detected with CT imaging (Figure 9F). AuNP were found within monocytes in the plaques of mice via transmission electron microscopy of the aortic sections, confirming that the in vivo CT imaging results corresponded to monocyte recruitment.

Cell Labeling Optimization. With increasing interest and recent advances in CT cell tracking techniques in various applications, more efforts have begun to focus on optimizing contrast generation. The limited number of CT cell tracking studies is partially due to CT's low sensitivity toward contrast media.[118] Despite the successful work mentioned above, the utility of CT cell tracking could be improved by thorough understanding of parameters for reaching maximum cell payloads without disrupting cell viability or function. The uptake pathway and cellular trafficking pattern of nanoparticles are of lesser concern in cell tracking, as long as the internalized nanoparticles generate detectable CT attenuation within the labeled cells; however, excretion of nanoparticles through efflux and exocytosis should be minimal to allow accurate and prolonged monitoring. Previous studies examining cellular uptake of AuNP have already demonstrated that physical and chemical parameters (i.e., size, shape, ligand coating) of nanoparticles and cell types play a critical role in uptake efficiency.[119−121] However, the main lesson from this prior work is that each parameter needs to be specifically optimized for individual applications. Furthermore, these studies mostly investigate cellular uptake for other biomedical applications, such as tumor intracellular delivery and autophagosome accumulation. Since their goals were not to investigate cellular uptake for CT cell tracking, vital information for cell tracking, such as labeled cell function preservation (e.g., viability, proliferation, function, and phenotype) and resulting CT attenuation from uptake of AuNP were often not studied. Furthermore, these investigations typically use incubation concentrations that are too low to be of much relevance to cell tracking applications. Recently, detailed investigations of incubation times, concentration, nanoparticle size, and ligand coating have been performed specifically for enhancing sensitivity of detection in CT cell tracking, which will be the focus of this section.

Betzer et al. examined the time and concentration dependence of AuNP uptake efficiency in different cell types, including human squamous carcinoma cancer cells (A-431), human immune cells (T-cells), and placenta-derived mesenchymal-like adherent stromal cells (PLX−PAD).[122] 10^6 cells of each type were incubated with 0.35 mg/mL 20-nm-diameter, glucose-coated AuNP for 1 h. TEM showed that nanoparticles were located in endosomes within the cells. Seeking to understand whether the cell uptake of the AuNP is driven by a temperature-sensitive process, incubations were done at 4 °C, which indeed resulted in a 38% reduction of uptake. To observe if AuNP labeling impaired cell functionality, different assessments were used for each cell type: cell density and cycle were tested for cancer cells; proliferation and cytokine secretion were tested for immune cells; and cell adhesion and medium-induced endothelial cell proliferation were tested for MSCs. The results showed minimal impairment in cell viability, proliferation, and biological function. Only slight impairments were observed for immune cells when incubated with high AuNP concentrations (>0.7 mg/mL) and for longer incubation times (2 h or more). The authors found that uptake of AuNP sharply increased up to 1 h for all cell types, but plateaued after this time. The effect of AuNP incubation concentration on cell uptake was also probed. Stem cells and cancer cells internalized AuNP in proportion to the incubation concentration (up to 1.05 mg/mL) without adverse effects on cell function and viability; however, uptake by immune cells did not increase when incubated at gold concentrations higher than 0.7 mg/mL. The difference in uptake behavior between these cell types is likely due to the smaller volume of the immune cells compared with the others.

In a recent study by Chhour et al., optimization of AuNP uptake by monocytes was pursued by examining effects of size and surface chemical functionality of AuNP on cellular uptake.[118] Spherical AuNP ranging from 15 to 150 nm in diameter were synthesized and coated with a variety of ligands, including straight-chain hydrocarbon ligands with distal carboxylic acid functional groups (i.e., 11-MUA and 16-MHA) and several different thiolated poly(ethylene glycol) (PEG) molecules that possessed different distal functional groups. In total, 44 different formulations were examined. The UV−vis absorption, hydrodynamic size, and surface charge of the various AuNP formulations were measured to confirm successful synthesis and ligand coating. The viability of monocytes treated with these different formulations of AuNP at gold concentrations of 0.1, 0.5, and 1.0 mg/mL was tested for 24 h. The majority of formulations in the 15 to 100 nm diameter range did not affect viability; however, viability was significantly reduced by several formulations at 150 nm in diameter, notably formulations coated with PEG that had amine functional groups. AuNP formulations that caused adverse effects on cell viability, as well as formulations that aggregated in cell culture media (since it would not be possible to separate these aggregates from labeled cells), were not studied further. Peak uptake was observed at 24 h of incubation with no significant increase in uptake after that time point. High cellular uptake was found for 15 to 50 nm AuNP coated with short chain carboxylic acid ligands (11-MUA, 16-MHA). AuNP coated with methoxy-PEG were taken up increasingly as their size increased, likely due to more contact with the cells from settling in the media. On the other hand, AuNP coated with PEG with a carboxylic acid end group had minimal uptake at 15 and 25 nm diameters, high uptake at 50 and 75 nm, and decreased uptake at 100 and 150 nm. This uptake trend was confirmed with TEM and CT imaging of the cells.

DOI: 10.1021/acs.bioconjchem.7b00194
Bioconjugate Chem. XXXX, XXX, XXX−XXX

The differing results between the work of Chhour et al. and Betzer et al. (e.g., uptake peaking at 24 h vs 1 h) underscores the need to optimize cell labeling conditions individually for specific nanoparticle formulations and cell types. We expect that more information on cell labeling optimization combined with improvements in CT technology and reconstruction software[14,123] will continue to improve detection of labeled cells in CT imaging via higher sensitivity and reduced radiation dose, facilitating the growing interest in using CT for cell tracking purposes.

DISCUSSION AND CONCLUSION

Thus far, the use of CT for cell tracking has been limited, due in part to the low sensitivity of CT. In the studies discussed above, high payloads were internalized in the cells (hundreds of pg/cell) to produce enough attenuation for detection.[118] This need for very high contrast agent payloads increases the possibility of affecting cell viability or function, which could result in misleading observations of cell migration and fate in the body. Furthermore, at such high concentrations, contrast agent that is released from the cells or is degraded could conceivably cause local tissue damage or systemic toxicity. Advances in nanoparticle formulations for cell labeling, as well as cell labeling techniques, could help address these issues. For example, techniques that have been used for labeling cells for other modalities, such as electroporation or antibody attachment, have not been explored. Furthermore, the development of new CT technology that allows better sensitivity and specificity of detection would be beneficial, and such technologies are emerging. For example, model-based iterative reconstruction techniques can suppress noise by a factor of 10, considerably increasing the sensitivity of contrast agent detection.[14] Photon counting CT allows specific detection of materials whose K-edge is in the 40−100 keV range.[63,124] This eliminates the need for laborious and error-prone pre- and post-injection image analysis. Such systems are now being tested in the clinic and small animal systems are commercially available.[125,126] The first studies where cell tracking is done using photon counting CT systems will likely be reported in the coming years.

Recent studies of nanoparticle protein coronas and their effects on colloidal stability and on nanoparticle−cell interaction (i.e., internalization, intracellular transportation, cytotoxicity upon protein degradation) reveal the significance of surrounding the nanoparticles with the "right" composition of proteins.[127−129] For cell tracking purposes, protein corona-dependent nanoparticle−cell interaction can be crucial to increase cellular uptake efficiency. Future studies may identify optimal protein compositions to improve cellular uptake while minimizing disruption of cell functionality. Improved uptake efficiency will also enable labeling of nonphagocytic cells, such as epithelial cells, endothelial cells, and fibroblasts, to broaden CT cell tracking applications.

The current reports of CT cell tracking use direct cell labeling. As mentioned above, this approach has several downsides, such the inability to distinguish live cells from dead, which can lead to misinterpretation of imaging results. Indirect cell labeling with reporter genes that can be expressed into enzymes, receptors, or transporters that facilitate accumulation of naturally existing CT attenuating elements in the human body (i.e., calcium and iodine) can potentially enable long-term CT cell tracking. Another downside of direct cell labeling is loss of signal due to exocytosis and cell division. Use of CT reporter genes or novel methods for cell retention of internalized nanoparticles (e.g., microtubule control) can prevent signal loss for long-term cell tracking.

For CT cell tracking, AuNP are by far the most widely studied class of contrast agent for labeling cells, due to biocompatibility, easily tailorable size and surface chemistry, and high attenuation in CT.[13] A potential issue for gold contrast agents is their cost; however, when scaling up from the mouse, only around a gram of gold will be needed for in vivo cell tracking in patients. Since the current price of gold is about $40/gram, CT cell tracking contrast agents based on this element will be affordable. Nevertheless, studies with labels synthesized from cheaper elements, such as bismuth, tantalum, lanthanum, or tungsten, would be of great interest and could further reduce the price of CT cell tracking. Methods to achieve nanoparticle clearance would be a further design improvement. For example, by synthesizing these nanoparticles to be smaller than the renal filtration threshold of approximately 6 nm, they can be rapidly cleared from the body to minimize or even eliminate nanoparticle retention.[130] Alternatively, nanoparticles based on bismuth, for example, can be designed to degrade for eventual excretion.[11,85] Development of multispectral CT will also allow simultaneous in vivo monitoring of multiple cell types by labeling them using contrast agents with different K-edge energies, which would further broaden the use of CT as a cell tracking imaging modality.

In summary, despite the low sensitivity of CT, cell tracking with this modality is possible. CT cell tracking has been demonstrated for microencapsulated pancreatic islet cells, as well as for a variety of immune, tumor, and stem cells, illustrating its broad applicability. The majority of reports of CT cell tracking have used AuNP, but given a plethora of recent reports on CT contrast agents, we expect that CT cell tracking will soon be performed with labels based on other elements. There is substantial room for further breakthroughs in this field, with topics such as cell loading optimization and reporter genes being largely unexplored. Given recent developments in both imaging systems and contrast agents, growing interest in using CT for cell tracking applications is anticipated.

AUTHOR INFORMATION

Corresponding Author

*E-mail: david.cormode@uphs.upenn.edu. Tel: 215-746-1382. Fax: 215-662-7868.

ORCID

Johoon Kim: 0000-0002-1138-5984
Peter Chhour: 0000-0001-7904-1195
Jessica Hsu: 0000-0002-3599-2834
David P. Cormode: 0000-0002-8391-9500

Notes

The authors declare no competing financial interest.

ACKNOWLEDGMENTS

We thank the NIH for funding that supported this work (R01 HL131557).

ABBREVIATIONS

CT, X-ray computed tomography; CNS, central nervous system; MRI, magnetic resonance imaging; SPIO, superparamagnetic iron oxide nanoparticles; QD, quantum dots; GFP, green fluorescent protein; BLI, bioluminescence imaging; PET, positron emission tomography; SPECT, single-photon

DOI: 10.1021/acs.bioconjchem.7b00194
Bioconjugate Chem. XXXX, XXX, XXX−XXX

emission computed tomography; PA, photoacoustic; HU, hounsfield unit; AuNP, gold nanoparticles; PLL, poly(L-lysine); PFC, perfluorocarbons; CIC, capsule-in-capsule; RITC, rhodamine B isothiocyanate; 11-MUA, 11-mercaptoundecanoic acid; 16-MHA, 16-mecaptohexadecanoic acid; PEI, poly(ethylenimine); 4-MB, 4-mercapto-1-butanol; MTEG, 11-mercaptoundecyl-tetra(ethylene glycol); TEM, transmission electron microscopy; PEG, poly(ethylene glycol)

REFERENCES

(1) Goodman, L. R. (2010) The Beatles, the Nobel Prize, and CT scanning of the chest. *Radiol Clin North Am. 48* (1), 1−7.

(2) Hounsfield, G. N. (1973) Computerized transverse axial scanning (tomography). 1. description of system. *Br. J. Radiol. 46* (552), 1016−22.

(3) OECD, Computed tomography (CT) exams (indicator) 2017.

(4) Chakravarty, S., Unold, J., Shuboni-Mulligan, D. D., Blanco-Fernandez, B., and Shapiro, E. M. (2016) Surface engineering of bismuth nanocrystals to counter dissolution. *Nanoscale 8* (27), 13217−22.

(5) Cheheltani, R., Ezzibdeh, R. M., Chhour, P., Pulaparthi, K., Kim, J., Jurcova, M., Hsu, J. C., Blundell, C., Litt, H. I., Ferrari, V. A., et al. (2016) Tunable, biodegradable gold nanoparticles as contrast agents for computed tomography and photoacoustic imaging. *Biomaterials 102*, 87−97.

(6) Cormode, D. P., Skajaa, T., van Schooneveld, M. M., Koole, R., Jarzyna, P., Lobatto, M. E., Calcagno, C., Barazza, A., Gordon, R. E., Zanzonico, P., et al. (2008) Nanocrystal core high-density lipoproteins: a multimodality contrast agent platform. *Nano Lett. 8* (11), 3715−23.

(7) Guay-Begin, A. A., Chevallier, P., Faucher, L., Turgeon, S., and Fortin, M. A. (2012) Surface modification of gadolinium oxide thin films and nanoparticles using poly(ethylene glycol)-phosphate. *Langmuir 28* (1), 774−782.

(8) Hwang, Y. H., and Lee, D. Y. (2012) Magnetic resonance imaging using heparin-coated superparamagnetic iron oxide nanoparticles for cell tracking in vivo. *Quant. Imaging Med. Surg. 2* (2), 118−23.

(9) Khan, S. A., Kanchanapally, R., Fan, Z., Beqa, L., Singh, A. K., Senapati, D., and Ray, P. C. (2012) A gold nanocage-CNT hybrid for targeted imaging and photothermal destruction of cancer cells. *Chem. Commun. (Cambridge, U. K.) 48* (53), 6711−3.

(10) Naha, P. C., Lau, K. C., Hsu, J. C., Hajfathalian, M., Mian, S., Chhour, P., Uppuluri, L., McDonald, E. S., Maidment, A. D., and Cormode, D. P. (2016) Gold silver alloy nanoparticles (GSAN): an imaging probe for breast cancer screening with dual-energy mammography or computed tomography. *Nanoscale 8* (28), 13740−54.

(11) Swy, E. R., Schwartz-Duval, A. S., Shuboni, D. D., Latourette, M. T., Mallet, C. L., Parys, M., Cormode, D. P., and Shapiro, E. M. (2014) Dual-modality, fluorescent, PLGA encapsulated bismuth nanoparticles for molecular and cellular fluorescence imaging and computed tomography. *Nanoscale 6* (21), 13104−12.

(12) Lee, D. E., Koo, H., Sun, I. C., Ryu, J. H., Kim, K., and Kwon, I. C. (2012) Multifunctional nanoparticles for multimodal imaging and theragnosis. *Chem. Soc. Rev. 41* (7), 2656−72.

(13) Mieszawska, A. J., Mulder, W. J., Fayad, Z. A., and Cormode, D. P. (2013) Multifunctional gold nanoparticles for diagnosis and therapy of disease. *Mol. Pharmaceutics 10* (3), 831−47.

(14) Bernstein, A. L., Dhanantwari, A., Jurcova, M., Cheheltani, R., Naha, P. C., Ivanc, T., Shefer, E., and Cormode, D. P. (2016) Improved sensitivity of computed tomography towards iodine and gold nanoparticle contrast agents via iterative reconstruction methods. *Sci. Rep. 6*, 26177.

(15) Pelc, N. J. (2014) Recent and future directions in CT imaging. *Ann. Biomed. Eng. 42* (2), 260−8.

(16) Kircher, M. F., Gambhir, S. S., and Grimm, J. (2011) Noninvasive cell-tracking methods. *Nat. Rev. Clin. Oncol. 8* (11), 677−88.

(17) Dai, H., Wang, Y., Lu, X., and Han, W. (2016) Chimeric antigen receptors modified T-Cells for cancer therapy. *J. Natl. Cancer Inst 108* (7), djv439.

(18) Cromer Berman, S. M., Walczak, P., and Bulte, J. W. (2011) Tracking stem cells using magnetic nanoparticles. *Wiley Interdiscip Rev. Nanomed Nanobiotechnol 3* (4), 343−55.

(19) Lee, A. R., Woo, S. K., Kang, S. K., Lee, S. Y., Lee, M. Y., Park, N. W., Song, S. H., Lee, S. Y., Nahm, S. S., Yu, J. E., et al. (2015) Adenovirus-mediated expression of human sodium-iodide symporter gene permits in vivo tracking of adipose tissue-derived stem cells in a canine myocardial infarction model. *Nucl. Med. Biol. 42* (7), 621−9.

(20) Joshi, P. P., Yoon, S. J., Chen, Y. S., Emelianov, S., and Sokolov, K. V. (2013) Development and optimization of near-IR contrast agents for immune cell tracking. *Biomed. Opt. Express 4* (11), 2609−18.

(21) Zhao, Y., Bower, A. J., Graf, B. W., Boppart, M. D., and Boppart, S. A. (2013) Imaging and tracking of bone marrow-derived immune and stem cells. *Methods Mol. Biol. 1052*, 57−76.

(22) Ji, X., Peng, F., Zhong, Y., Su, Y., Jiang, X., Song, C., Yang, L., Chu, B., Lee, S. T., and He, Y. (2015) Highly fluorescent, photostable, and ultrasmall silicon drug nanocarriers for long-term tumor cell tracking and in-vivo cancer therapy. *Adv. Mater. 27* (6), 1029−34.

(23) Srivastava, A. K., and Bulte, J. W. (2014) Seeing stem cells at work in vivo. *Stem Cell Rev. 10* (1), 127−44.

(24) Landazuri, N., Levit, R. D., Joseph, G., Ortega-Legaspi, J. M., Flores, C. A., Weiss, D., Sambanis, A., Weber, C. J., Safley, S. A., and Taylor, W. R. (2016) Alginate microencapsulation of human mesenchymal stem cells as a strategy to enhance paracrine-mediated vascular recovery after hindlimb ischaemia. *J. Tissue Eng. Regener. Med. 10* (3), 222−32.

(25) Kim, J., Shapiro, L., and Flynn, A. (2015) The clinical application of mesenchymal stem cells and cardiac stem cells as a therapy for cardiovascular disease. *Pharmacol. Ther. 151*, 8−15.

(26) Sullivan, R., Duncan, K., Dailey, T., Kaneko, Y., Tajiri, N., and Borlongan, C. V. (2015) A possible new focus for stroke treatment - migrating stem cells. *Expert Opin. Biol. Ther. 15* (7), 949−58.

(27) Wolff, E. F., Mutlu, L., Massasa, E. E., Elsworth, J. D., Eugene Redmond, D., Jr., and Taylor, H. S. (2015) Endometrial stem cell transplantation in MPTP- exposed primates: an alternative cell source for treatment of Parkinson's disease. *J. Cell Mol. Med. 19* (1), 249−56.

(28) Gonzalez, C., Bonilla, S., Flores, A. I., Cano, E., and Liste, I. (2016) An update on human stem cell-based therapy in Parkinson's disease. *Curr. Stem Cell Res. Ther. 11* (7), 561−8.

(29) Xie, C., Liu, Y. Q., Guan, Y. T., and Zhang, G. X. (2016) Induced stem cells as a novel multiple sclerosis therapy. *Curr. Stem Cell Res. Ther. 11* (4), 313−20.

(30) Xu, C., Mu, L., Roes, I., Miranda-Nieves, D., Nahrendorf, M., Ankrum, J. A., Zhao, W., and Karp, J. M. (2011) Nanoparticle-based monitoring of cell therapy. *Nanotechnology 22* (49), 494001.

(31) Long, C. M., and Bulte, J. W. (2009) In vivo tracking of cellular therapeutics using magnetic resonance imaging. *Expert Opin. Biol. Ther. 9* (3), 293−306.

(32) Villa, C., Erratico, S., Razini, P., Fiori, F., Rustichelli, F., Torrente, Y., and Belicchi, M. (2010) Stem cell tracking by nanotechnologies. *Int. J. Mol. Sci. 11* (3), 1070−81.

(33) Thorek, D. L., Tsao, P. Y., Arora, V., Zhou, L., Eisenberg, R. A., and Tsourkas, A. (2010) In vivo, multimodal imaging of B cell distribution and response to antibody immunotherapy in mice. *PLoS One 5* (5), e10655.

(34) Kang, S., Lee, H. W., Jeon, Y. H., Singh, T. D., Choi, Y. J., Park, J. Y., Kim, J. S., Lee, H., Hong, K. S., Lee, I., et al. (2015) Combined fluorescence and magnetic resonance imaging of primary macrophage migration to sites of acute inflammation using near-infrared fluorescent magnetic nanoparticles. *Mol. Imaging Biol. 17* (5), 643−51.

(35) Riechelmann, H., Wiesneth, M., Schauwecker, P., Reinhardt, P., Gronau, S., Schmitt, A., Schroen, C., Atz, J., and Schmitt, M. (2007) Adoptive therapy of head and neck squamous cell carcinoma with antibody coated immune cells: a pilot clinical trial. *Cancer Immunol. Immunother. 56* (9), 1397−406.

DOI: 10.1021/acs.bioconjchem.7b00194
Bioconjugate Chem. XXXX, XXX, XXX−XXX

(36) Khammari, A., Nguyen, J. M., Saint-Jean, M., Knol, A. C., Pandolfino, M. C., Quereux, G., Brocard, A., Peuvrel, L., Saiagh, S., Bataille, V., et al. (2015) Adoptive T cell therapy combined with intralesional administrations of TG1042 (adenovirus expressing interferon-gamma) in metastatic melanoma patients. *Cancer Immunol. Immunother. 64* (7), 805−15.
(37) Arifin, D. R., Long, C. M., Gilad, A. A., Alric, C., Roux, S., Tillement, O., Link, T. W., Arepally, A., and Bulte, J. W. (2011) Trimodal gadolinium-gold microcapsules containing pancreatic islet cells restore normoglycemia in diabetic mice and can be tracked by using US, CT, and positive-contrast MR imaging. *Radiology 260* (3), 790−8.
(38) Saudek, F., Brogren, C. H., and Manohar, S. (2008) Imaging the beta-cell mass: why and how. *Rev. Diabet Stud 5* (1), 6−12.
(39) Lien, Z. Y., Hsu, T. C., Liu, K. K., Liao, W. S., Hwang, K. C., and Chao, J. I. (2012) Cancer cell labeling and tracking using fluorescent and magnetic nanodiamond. *Biomaterials 33* (26), 6172−85.
(40) van der Horst, G., van Asten, J. J., Figdor, A., van den Hoogen, C., Cheung, H., Bevers, R. F., Pelger, R. C., and van der Pluijm, G. (2011) Real-time cancer cell tracking by bioluminescence in a preclinical model of human bladder cancer growth and metastasis. *Eur. Urol. 60* (2), 337−43.
(41) Bulte, J. W. (2009) In vivo MRI cell tracking: clinical studies. *AJR, Am. J. Roentgenol. 193* (2), 314−25.
(42) Meir, R., Motiei, M., and Popovtzer, R. (2014) Gold nanoparticles for in vivo cell tracking. *Nanomedicine (London, U. K.) 9* (13), 2059−69.
(43) de Vries, I. J., Lesterhuis, W. J., Barentsz, J. O., Verdijk, P., van Krieken, J. H., Boerman, O. C., Oyen, W. J., Bonenkamp, J. J., Boezeman, J. B., Adema, G. J., et al. (2005) Magnetic resonance tracking of dendritic cells in melanoma patients for monitoring of cellular therapy. *Nat. Biotechnol. 23* (11), 1407−13.
(44) Kazuma, S. M., Sultan, D., Zhao, Y., Detering, L., You, M., Luehmann, H. P., Abdalla, D. S., and Liu, Y. (2015) Recent advances of radionuclide-based molecular imaging of atherosclerosis. *Curr. Pharm. Des. 21* (36), 5267−76.
(45) Hahn, M. A., Singh, A. K., Sharma, P., Brown, S. C., and Moudgil, B. M. (2011) Nanoparticles as contrast agents for in-vivo bioimaging: current status and future perspectives. *Anal. Bioanal. Chem. 399* (1), 3−27.
(46) Acton, P. D., and Zhou, R. (2005) Imaging reporter genes for cell tracking with PET and SPECT. *Q. J. Nucl. Med. Mol. Imaging 49* (4), 349−60.
(47) Kogan, F., Fan, A. P., and Gold, G. E. (2016) Potential of PET-MRI for imaging of non-oncologic musculoskeletal disease. *Quant Imaging Med. Surg 6* (6), 756−71.
(48) Jung, W., Jang, J. Y., Kang, M. J., Chang, Y. R., Shin, Y. C., Chang, J., and Kim, S. W. (2016) The clinical usefulness of 18F-fluorodeoxyglucose positron emission tomography-computed tomography (PET-CT) in follow-up of curatively resected pancreatic cancer patients. *HPB (Oxford) 18* (1), 57−64.
(49) Fu, Y., Azene, N., Xu, Y., and Kraitchman, D. L. (2011) Tracking stem cells for cardiovascular applications in vivo: focus on imaging techniques. *Imaging Med. 3* (4), 473−86.
(50) Yaghoubi, S. S., Jensen, M. C., Satyamurthy, N., Budhiraja, S., Paik, D., Czernin, J., and Gambhir, S. S. (2009) Noninvasive detection of therapeutic cytolytic T cells with 18F-FHBG PET in a patient with glioma. *Nat. Clin. Pract. Oncol. 6* (1), 53−8.
(51) Emelianov, S. Y., Li, P. C., and O'Donnell, M. (2009) Photoacoustics for molecular imaging and therapy. *Phys. Today 62* (8), 34−9.
(52) Weber, J., Beard, P. C., and Bohndiek, S. E. (2016) Contrast agents for molecular photoacoustic imaging. *Nat. Methods 13* (8), 639−50.
(53) Jokerst, J. V., Thangaraj, M., Kempen, P. J., Sinclair, R., and Gambhir, S. S. (2012) Photoacoustic imaging of mesenchymal stem cells in living mice via silica-coated gold nanorods. *ACS Nano 6* (7), 5920−30.
(54) Nam, S. Y., Ricles, L. M., Suggs, L. J., and Emelianov, S. Y. (2012) In vivo ultrasound and photoacoustic monitoring of mesenchymal stem cells labeled with gold nanotracers. *PLoS One 7* (5), e37267.
(55) Cui, W., Tavri, S., Benchimol, M. J., Itani, M., Olson, E. S., Zhang, H., Decyk, M., Ramirez, R. G., Barback, C. V., Kono, Y., et al. (2013) Neural progenitor cells labeling with microbubble contrast agent for ultrasound imaging in vivo. *Biomaterials 34* (21), 4926−35.
(56) Shapiro, M. G., Goodwill, P. W., Neogy, A., Yin, M., Foster, F. S., Schaffer, D. V., and Conolly, S. M. (2014) Biogenic gas nanostructures as ultrasonic molecular reporters. *Nat. Nanotechnol. 9* (4), 311−6.
(57) Cormode, D. P., Naha, P. C., and Fayad, Z. A. (2014) Nanoparticle contrast agents for computed tomography: a focus on micelles. *Contrast Media Mol. Imaging 9* (1), 37−52.
(58) Lee, N., Choi, S. H., and Hyeon, T. (2013) Nano-sized CT contrast agents. *Adv. Mater. 25* (19), 2641−60.
(59) Danad, I., Fayad, Z. A., Willemink, M. J., and Min, J. K. (2015) New applications of cardiac computed tomography: dual-energy, spectral, and molecular CT Imaging. *JACC Cardiovasc Imaging 8* (6), 710−23.
(60) Heismann, B. S. B., and Flohr, T. (2012) *Spectral computed tomography*, pp 5−12, Chapter 2, Society of Photo-Optical Instrumentation Engineers (SPIE) PRESS, Bellingham, WA.
(61) Halpern, E. J., Gingold, E. L., White, H., and Read, K. (2014) Evaluation of coronary artery image quality with knowledge-based iterative model reconstruction. *Acad. Radiol 21* (6), 805−11.
(62) Bardo, D. M., and Brown, P. (2008) Cardiac multidetector computed tomography: basic physics of image acquisition and clinical applications. *Curr. Cardiol. Rev. 4* (3), 231−43.
(63) Cormode, D. P., Roessl, E., Thran, A., Skajaa, T., Gordon, R. E., Schlomka, J. P., Fuster, V., Fisher, E. A., Mulder, W. J., Proksa, R., et al. (2010) Atherosclerotic plaque composition: analysis with multicolor CT and targeted gold nanoparticles. *Radiology 256* (3), 774−82.
(64) Boussel, L., Coulon, P., Thran, A., Roessl, E., Martens, G., Sigovan, M., and Douek, P. (2014) Photon counting spectral CT component analysis of coronary artery atherosclerotic plaque samples. *Br. J. Radiol. 87* (1040), 20130798.
(65) Kalluri, K. S., Mahd, M., and Glick, S. J. (2013) Investigation of energy weighting using an energy discriminating photon counting detector for breast CT. *Med. Phys. 40* (8), 081923.
(66) Oliva, M. R., Erturk, S. M., Ichikawa, T., Rocha, T., Ros, P. R., Silverman, S. G., and Mortele, K. J. (2015) Gastrointestinal tract wall visualization and distention during abdominal and pelvic multidetector CT with a neutral barium sulphate suspension: comparison with positive barium sulphate suspension and with water. *JBR-BTR 95* (4), 237−42.
(67) Kurihara, O., Takano, M., Uchiyama, S., Fukuizumi, I., Shimura, T., Matsushita, M., Komiyama, H., Inami, T., Murakami, D., Munakata, R., et al. (2015) Microvascular resistance in response to iodinated contrast media in normal and functionally impaired kidneys. *Clin. Exp. Pharmacol. Physiol. 42* (12), 1245−50.
(68) Pasternak, J. J., and Williamson, E. E. (2012) Clinical pharmacology, uses, and adverse reactions of iodinated contrast agents: a primer for the non-radiologist. *Mayo Clin. Proc. 87* (4), 390−402.
(69) Sendeski, M. M., Persson, A. B., Liu, Z. Z., Busch, J. F., Weikert, S., Persson, P. B., Hippenstiel, S., and Patzak, A. (2012) Iodinated contrast media cause endothelial damage leading to vasoconstriction of human and rat vasa recta. *Am. J. Physiol Renal Physiol 303* (12), F1592−8.
(70) Liu, Z. Z., Schmerbach, K., Lu, Y., Perlewitz, A., Nikitina, T., Cantow, K., Seeliger, E., Persson, P. B., Patzak, A., Liu, R., et al. (2014) Iodinated contrast media cause direct tubular cell damage, leading to oxidative stress, low nitric oxide, and impairment of tubuloglomerular feedback. *Am. J. Physiol Renal Physiol 306* (8), F864−72.
(71) Bottinor, W., Polkampally, P., and Jovin, I. (2013) Adverse reactions to iodinated contrast media. *Int. J. Angiol. 22* (3), 149−54.

DOI: 10.1021/acs.bioconjchem.7b00194
Bioconjugate Chem. XXXX, XXX, XXX−XXX

(72) Cole, L. E., Ross, R. D., Tilley, J. M., Vargo-Gogola, T., and Roeder, R. K. (2015) Gold nanoparticles as contrast agents in x-ray imaging and computed tomography. *Nanomedicine (London, U. K.) 10* (2), 321−41.
(73) Liu, Y., Ai, K., and Lu, L. (2012) Nanoparticulate X-ray computed tomography contrast agents: from design validation to in vivo applications. *Acc. Chem. Res. 45* (10), 1817−27.
(74) Pan, D., Schirra, C. O., Wickline, S. A., and Lanza, G. M. (2014) Multicolor computed tomographic molecular imaging with noncrystalline high-metal-density nanobeacons. *Contrast Media Mol. Imaging 9* (1), 13−25.
(75) Chinen, A. B., Guan, C. M., Ferrer, J. R., Barnaby, S. N., Merkel, T. J., and Mirkin, C. A. (2015) Nanoparticle probes for the detection of cancer biomarkers, cells, and tissues by fluorescence. *Chem. Rev. 115* (19), 10530−74.
(76) Tepel, M., Aspelin, P., and Lameire, N. (2006) Contrast-induced nephropathy: a clinical and evidence-based approach. *Circulation 113* (14), 1799−1806.
(77) Brockow, K., and Sanchez-Borges, M. (2014) Hypersensitivity to contrast media and dyes. *Immunol. Allergy Clin. North Am. 34* (3), 547−64.
(78) Abadeer, N. S., Fulop, G., Chen, S., Kall, M., and Murphy, C. J. (2015) Interactions of bacterial lipopolysaccharides with gold nanorod surfaces investigated by refractometric sensing. *ACS Appl. Mater. Interfaces 7* (44), 24915−25.
(79) Li, M., Li, L., Zhan, C., and Kohane, D. S. (2016) Core-shell nanostars for multimodal therapy and imaging. *Theranostics 6* (13), 2306−13.
(80) Kim, W., Kim, N., Park, J. W., and Kim, Z. H. (2016) Nanostar probes for tip-enhanced spectroscopy. *Nanoscale 8* (2), 987−94.
(81) Liu, X. L., Liang, S., Nan, F., Yang, Z. J., Yu, X. F., Zhou, L., Hao, Z. H., and Wang, Q. Q. (2013) Solution-dispersible Au nanocube dimers with greatly enhanced two-photon luminescence and SERS. *Nanoscale 5* (12), 5368−74.
(82) Jia, F., Liu, X., Li, L., Mallapragada, S., Narasimhan, B., and Wang, Q. (2013) Multifunctional nanoparticles for targeted delivery of immune activating and cancer therapeutic agents. *J. Controlled Release 172* (3), 1020−34.
(83) Ghaghada, K. B., Sato, A. F., Starosolski, Z. A., Berg, J., and Vail, D. M. (2016) Computed tomography imaging of solid tumors using a liposomal-iodine contrast agent in companion dogs with naturally occurring cancer. *PLoS One 11* (3), e0152718.
(84) Thakor, A. S., Jokerst, J., Zavaleta, C., Massoud, T. F., and Gambhir, S. S. (2011) Gold nanoparticles: a revival in precious metal administration to patients. *Nano Lett. 11* (10), 4029−36.
(85) Naha, P. C., Al Zaki, A., Hecht, E., Chorny, M., Chhour, P., Blankemeyer, E., Yates, D. M., Witschey, W. R., Litt, H. I., Tsourkas, A., et al. (2014) Dextran coated bismuth-iron oxide nanohybrid contrast agents for computed tomography and magnetic resonance imaging. *J. Mater. Chem. B 2* (46), 8239−48.
(86) Ashton, J. R., West, J. L., and Badea, C. T. (2015) In vivo small animal micro-CT using nanoparticle contrast agents. *Front. Pharmacol. 6*, 256.
(87) von Maltzahn, G., Park, J. H., Agrawal, A., Bandaru, N. K., Das, S. K., Sailor, M. J., and Bhatia, S. N. (2009) Computationally guided photothermal tumor therapy using long-circulating gold nanorod antennas. *Cancer Res. 69* (9), 3892−900.
(88) Zhu, J., Zhou, L., and XingWu, F. (2006) Tracking neural stem cells in patients with brain trauma. *N. Engl. J. Med. 355* (22), 2376−8.
(89) Callera, F., and de Melo, C. M. (2007) Magnetic resonance tracking of magnetically labeled autologous bone marrow CD34+ cells transplanted into the spinal cord via lumbar puncture technique in patients with chronic spinal cord injury: CD34+ cells' migration into the injured site. *Stem Cells Dev. 16* (3), 461−6.
(90) Toso, C., Vallee, J. P., Morel, P., Ris, F., Demuylder-Mischler, S., Lepetit-Coiffe, M., Marangon, N., Saudek, F., James Shapiro, A. M., Bosco, D., et al. (2008) Clinical magnetic resonance imaging of pancreatic islet grafts after iron nanoparticle labeling. *Am. J. Transplant. 8* (3), 701−6.
(91) Muller, C., Zielinski, C. C., Linkesch, W., Ludwig, H., and Sinzinger, H. (1989) In vivo tracing of indium-111 oxine-labeled human peripheral blood mononuclear cells in patients with lymphatic malignancies. *J. Nucl. Med. 30* (6), 1005−11.
(92) Arifin, D. R., Kedziorek, D. A., Fu, Y., Chan, K. W., McMahon, M. T., Weiss, C. R., Kraitchman, D. L., and Bulte, J. W. (2013) Microencapsulated cell tracking. *NMR Biomed. 26* (7), 850−9.
(93) Jitraruch, S., Dhawan, A., Hughes, R. D., Filippi, C., Soong, D., Philippeos, C., Lehec, S. C., Heaton, N. D., Longhi, M. S., and Mitry, R. R. (2014) Alginate microencapsulated hepatocytes optimized for transplantation in acute liver failure. *PLoS One 9* (12), e113609.
(94) Hosseini, S. M., Sharafkhah, A., Koohi-Hosseinabadi, O., and Semsar-Kazerooni, M. (2016) Transplantation of neural stem cells cultured in alginate scaffold for spinal cord injury in rats. *Asian Spine J. 10* (4), 611−8.
(95) Lim, F., and Sun, A. M. (1980) Microencapsulated islets as bioartificial endocrine pancreas. *Science 210* (4472), 908−10.
(96) Tuch, B. E., Keogh, G. W., Williams, L. J., Wu, W., Foster, J. L., Vaithilingam, V., and Philips, R. (2009) Safety and viability of microencapsulated human islets transplanted into diabetic humans. *Diabetes Care 32* (10), 1887−9.
(97) Soon-Shiong, P., Heintz, R. E., Merideth, N., Yao, Q. X., Yao, Z., Zheng, T., Murphy, M., Moloney, M. K., Schmehl, M., Harris, M., et al. (1994) Insulin independence in a type 1 diabetic patient after encapsulated islet transplantation. *Lancet 343* (8903), 950−1.
(98) Arifin, D. R., Manek, S., Call, E., Arepally, A., and Bulte, J. W. (2012) Microcapsules with intrinsic barium radiopacity for immunoprotection and X-ray/CT imaging of pancreatic islet cells. *Biomaterials 33* (18), 4681−9.
(99) Astolfo, A., Qie, F., Kibleur, A., Hao, X., Menk, R. H., Arfelli, F., Rigon, L., Hinton, T. M., Wickramaratna, M., Tan, T., et al. (2014) A simple way to track single gold-loaded alginate microcapsules using X-ray CT in small animal longitudinal studies. *Nanomedicine (N. Y., NY, U. S.) 10* (8), 1821−8.
(100) Barnett, B. P., Ruiz-Cabello, J., Hota, P., Liddell, R., Walczak, P., Howland, V., Chacko, V. P., Kraitchman, D. L., Arepally, A., and Bulte, J. W. (2011) Fluorocapsules for improved function, immunoprotection, and visualization of cellular therapeutics with MR, US, and CT imaging. *Radiology 258* (1), 182−91.
(101) Barnett, B. P., Ruiz-Cabello, J., Hota, P., Ouwerkerk, R., Shamblott, M. J., Lauzon, C., Walczak, P., Gilson, W. D., Chacko, V. P., Kraitchman, D. L., et al. (2011) Use of perfluorocarbon nanoparticles for non-invasive multimodal cell tracking of human pancreatic islets. *Contrast Media Mol. Imaging 6* (4), 251−9.
(102) Kim, J., Arifin, D. R., Muja, N., Kim, T., Gilad, A. A., Kim, H., Arepally, A., Hyeon, T., and Bulte, J. W. (2011) Multifunctional capsule-in-capsules for immunoprotection and trimodal imaging. *Angew. Chem., Int. Ed. 50* (10), 2317−21.
(103) Astolfo, A., Schultke, E., Menk, R. H., Kirch, R. D., Juurlink, B. H., Hall, C., Harsan, L. A., Stebel, M., Barbetta, D., Tromba, G., et al. (2013) In vivo visualization of gold-loaded cells in mice using X-ray computed tomography. *Nanomedicine (N. Y., NY, U. S.) 9* (2), 284−92.
(104) Hall, C. J., Schultke, E., Rigon, L., Ataelmannan, K., Rigley, S., Menk, R., Arfelli, F., Tromba, G., Pearson, S., Wilkinson, S., et al. (2008) Synchrotron-based in vivo tracking of implanted mammalian cells. *Eur. J. Radiol. 68* (3), S156.
(105) Menk, R. H., Schultke, E., Hall, C., Arfelli, F., Astolfo, A., Rigon, L., Round, A., Ataelmannan, K., MacDonald, S. R., and Juurlink, B. H. (2011) Gold nanoparticle labeling of cells is a sensitive method to investigate cell distribution and migration in animal models of human disease. *Nanomedicine (N. Y., NY, U. S.) 7* (5), 647−54.
(106) Schultke, E., Menk, R., Pinzer, B., Astolfo, A., Stampanoni, M., Arfelli, F., Harsan, L. A., and Nikkhah, G. (2014) Single-cell resolution in high-resolution synchrotron X-ray CT imaging with gold nanoparticles. *J. Synchrotron Radiat. 21* (1), 242−50.
(107) Torrente, Y., Gavina, M., Belicchi, M., Fiori, F., Komlev, V., Bresolin, N., and Rustichelli, F. (2006) High-resolution X-ray microtomography for three-dimensional visualization of human stem cell muscle homing. *FEBS Lett. 580* (24), 5759−64.

DOI: 10.1021/acs.bioconjchem.7b00194
Bioconjugate Chem. XXXX, XXX, XXX−XXX

(108) Corot, C., Robert, P., Idee, J. M., and Port, M. (2006) Recent advances in iron oxide nanocrystal technology for medical imaging. *Adv. Drug Delivery Rev. 58* (14), 1471−504.
(109) Rustad, K. C., and Gurtner, G. C. (2012) Mesenchymal stem cells home to sites of injury and inflammation. *Adv. Wound Care (New Rochelle) 1* (4), 147−52.
(110) Kim, T., Lee, N., Arifin, D. R., Shats, I., Janowski, M., Walczak, P., Hyeon, T., and Bulte, J. W. (2017) In vivo micro-CT imaging of human mesenchymal stem cells labeled with gold-poly-l-lysine nanocomplexes. *Adv. Funct. Mater. 27* (3), 1604213.
(111) Betzer, O., Shwartz, A., Motiei, M., Kazimirsky, G., Gispan, I., Damti, E., Brodie, C., Yadid, G., and Popovtzer, R. (2014) Nanoparticle-based CT imaging technique for longitudinal and quantitative stem cell tracking within the brain: application in neuropsychiatric disorders. *ACS Nano 8* (9), 9274−85.
(112) Philippi, C. L., Motzkin, J. C., Pujara, M. S., and Koenigs, M. (2015) Subclinical depression severity is associated with distinct patterns of functional connectivity for subregions of anterior cingulate cortex. *J. Psychiatr. Res. 71*, 103−11.
(113) Tripp, A., Oh, H., Guilloux, J. P., Martinowich, K., Lewis, D. A., and Sibille, E. (2012) Brain-derived neurotrophic factor signaling and subgenual anterior cingulate cortex dysfunction in major depressive disorder. *Am. J. Psychiatry 169* (11), 1194−202.
(114) Meir, R., Betzer, O., Motiei, M., Kronfeld, N., Brodie, C., and Popovtzer, R. (2017) Design principles for noninvasive, longitudinal and quantitative cell tracking with nanoparticle-based CT imaging. *Nanomedicine (N. Y., NY, U. S.) 13* (2), 421−29.
(115) Meir, R., Shamalov, K., Betzer, O., Motiei, M., Horovitz-Fried, M., Yehuda, R., Popovtzer, A., Popovtzer, R., and Cohen, C. J. (2015) Nanomedicine for cancer immunotherapy: tracking cancer-specific T-cells in vivo with gold nanoparticles and CT imaging. *ACS Nano 9* (6), 6363−72.
(116) Chhour, P., Naha, P. C., O'Neill, S. M., Litt, H. I., Reilly, M. P., Ferrari, V. A., and Cormode, D. P. (2016) Labeling monocytes with gold nanoparticles to track their recruitment in atherosclerosis with computed tomography. *Biomaterials 87*, 93−103.
(117) Ley, K., Miller, Y. I., and Hedrick, C. C. (2011) Monocyte and macrophage dynamics during atherogenesis. *Arterioscler., Thromb., Vasc. Biol. 31* (7), 1506−16.
(118) Chhour, P., Kim, J., Benardo, B., Tovar, A., Mian, S., Litt, H. I., Ferrari, V. A., and Cormode, D. P. (2017) Effect of gold nanoparticle size and coating on labeling monocytes for CT tracking. *Bioconjugate Chem. 28* (1), 260−69.
(119) Chithrani, B. D., Ghazani, A. A., and Chan, W. C. (2006) Determining the size and shape dependence of gold nanoparticle uptake into mammalian cells. *Nano Lett. 6* (4), 662−8.
(120) Ma, X., Wu, Y., Jin, S., Tian, Y., Zhang, X., Zhao, Y., Yu, L., and Liang, X. J. (2011) Gold nanoparticles induce autophagosome accumulation through size-dependent nanoparticle uptake and lysosome impairment. *ACS Nano 5* (11), 8629−39.
(121) Shilo, M., Sharon, A., Baranes, K., Motiei, M., Lellouche, J. P., and Popovtzer, R. (2015) The effect of nanoparticle size on the probability to cross the blood-brain barrier: an in-vitro endothelial cell model. *J. Nanobiotechnol. 13*, 19.
(122) Betzer, O., Meir, R., Dreifuss, T., Shamalov, K., Motiei, M., Shwartz, A., Baranes, K., Cohen, C. J., Shraga-Heled, N., Ofir, R., et al. (2015) In-vitro optimization of nanoparticle-cell labeling protocols for in-vivo cell tracking applications. *Sci. Rep. 5*, 15400.
(123) Astolfo, A., Arfelli, F., Schultke, E., James, S., Mancini, L., and Menk, R. H. (2013) A detailed study of gold-nanoparticle loaded cells using X-ray based techniques for cell-tracking applications with single-cell sensitivity. *Nanoscale 5* (8), 3337−45.
(124) Allijn, I. E., Leong, W., Tang, J., Gianella, A., Mieszawska, A. J., Fay, F., Ma, G., Russell, S., Callo, C. B., Gordon, R. E., et al. (2013) Gold nanocrystal labeling allows low-density lipoprotein imaging from the subcellular to macroscopic level. *ACS Nano 7* (11), 9761−70.
(125) Muenzel, D., Bar-Ness, D., Roessl, E., Blevis, I., Bartels, M., Fingerle, A. A., Ruschke, S., Coulon, P., Daerr, H., and Kopp, F. K. (2016) Spectral photon-counting CT: initial experience with dual-contrast agent K-edge colonography. *Radiology*, 160890.
(126) MARS: Medipix All Resolution System http://www.marsbioimaging.com/mars/ (accessed March 7th).
(127) Wan, S., Kelly, P. M., Mahon, E., Stockmann, H., Rudd, P. M., Caruso, F., Dawson, K. A., Yan, Y., and Monopoli, M. P. (2015) The "sweet" side of the protein corona: effects of glycosylation on nanoparticle-cell interactions. *ACS Nano 9* (2), 2157−66.
(128) Mirshafiee, V., Kim, R., Park, S., Mahmoudi, M., and Kraft, M. L. (2016) Impact of protein pre-coating on the protein corona composition and nanoparticle cellular uptake. *Biomaterials 75*, 295−304.
(129) Ma, Z., Bai, J., and Jiang, X. (2015) Monitoring of the enzymatic degradation of protein corona and evaluating the accompanying cytotoxicity of nanoparticles. *ACS Appl. Mater. Interfaces 7* (32), 17614−22.
(130) Choi, H. S., Liu, W., Misra, P., Tanaka, E., Zimmer, J. P., Itty Ipe, B., Bawendi, M. G., and Frangioni, J. V. (2007) Renal clearance of quantum dots. *Nat. Biotechnol. 25* (10), 1165−70.

DOI: 10.1021/acs.bioconjchem.7b00194
Bioconjugate Chem. XXXX, XXX, XXX−XXX